# Differential Metabolic Sensitivity of mTORC1- and mTORC2-Dependent Overgrowth

Maelle Devilliers[1], Damien Garrido[1,‡], Mickael Poidevin[1], Thomas Rubin[1,§], Arnaud Le Rouzic[2], and Jacques Montagne[1,*]

[1] Institute for Integrative Biology of the Cell (I2BC), CNRS, Université Paris-Sud, CEA, F-91190, Gif-sur-Yvette, France

[2] Laboratoire Evolution, Génomes, Comportement et Ecologie, CNRS, Université Paris-Sud, UMR 9191, F-91190, Gif-sur-Yvette, France

* Correspondence: Jacques.MONTAGNE@i2bc.paris-saclay.fr

‡ Present address: IRIC, Université de Montréal, Montréal, Québec H3T 1J4, Canada

§ Present address: Institut Curie, CNRS UMR 3215 / INSERM U-934, F-75248 Paris Cedex 5

Key words: Lipogenesis, Glycolysis, cell-autonomous effect, homeostasis

Short title: Metabolism and mTOR-induced overgrowth

**ABSTRACT**

The protein kinase mTOR is implicated in metabolic-related diseases and chiefly controls organismal growth and homeostasis in response to nutrients. Activation of mTOR promotes cell growth and enhances a glycolytic/lipogenic axis, suggesting that this metabolic axis is required to sustain mTOR-dependent growth. Here, we used *Drosophila* genetics to investigate this functional link both at the organismal and cell-autonomous levels. mTOR is present in two distinct complexes mTORC1 and mTORC2, which can be independently modulated in most *Drosophila* tissues. We confirm this independency in the fat body, the organ that fulfils hepatic and adipose functions. We show that ubiquitous mTOR over-activation affects carbohydrate and lipid metabolism, supporting the use of *Drosophila* as a powerful model to study the link between mTOR and metabolism. We show that targeted glycolytic or lipogenic restriction in fat body cells exclusively impedes mTORC2-induced overgrowth. Additionally, ubiquitous deficiency of lipogenesis (*FASN* mutants) results in a drop in mTORC1 but not mTORC2 signaling, whereas, at the cell-autonomous level, lipogenesis deficiency in fat body cells affects neither mTORC1 nor mTORC2 activity. These findings thus, reveal differential metabolic sensitivity of mTORC1- and mTORC2-dependent overgrowth. Furthermore, they suggest that local metabolic defects may elicit compensatory pathways between neighboring cells, whereas enzyme knockdown in the whole organism results in animal death. Importantly, our study weakens the use of single inhibitors to fight mTOR-related diseases and strengthens the use of drug combination and selective tissue-targeting.

## AUTHOR SUMMARY

Cell growth is essential for animal development but is also deregulated in several human diseases including cancers. The mTOR signaling network controls cell growth in response to nutrients and growth factors. mTOR stimulation has been shown to promote basal metabolism, including the glycolytic/lipogenic axis, which is essential to provide energetic cofactors and building blocks to sustain cell growth. However, the requirement this metabolic axis for mTOR-dependent growth has been poorly investigated yet. To address this issue, we used *Drosophila* genetics and focused on the fat tissue that fulfils hepatic and adipose functions. Surprisingly, in mosaic animals, where only a few cells were genetically stimulated for mTOR, we observed that metabolic knockdown only moderates cell overgrowth. Additionally, this growth restriction operates for only one of the two mTOR signaling branches, suggesting that mTOR-dependent compensatory processes operate to circumvent metabolic defects. Given that ubiquitous knockdown of this metabolic axis is essential for juvenile development and adult survival, our study reveals that metabolic restriction is unlikely sufficient to counteract overgrowth disorders.

## INTRODUCTION

Growth of a multicellular organism is coordinated by signaling pathways that adjust intracellular processes to environmental changes. These signaling pathways include the mTOR (mechanistic Target Of Rapamycin) regulatory network that integrates the growth factor response as well as the nutritional and energetic status [1-7]. This network consists in two signaling branches in which the mTOR protein kinase is present in two distinct complexes, mTORC1 and mTORC2 that comprise raptor and rictor, respectively [8, 9]. Both mTORC1 and mTORC2 promote basal cellular functions, thereby providing building blocks to sustain cellular growth. However, despite a plethora of studies on mTORC1/2 signaling and functions, the requirement of basal metabolism—glycolytic/lipogenic axis— for mTOR-dependent cell growth has not been systematically investigated. The *Drosophila* model provides a powerful genetic system to address these issues [10], since both the intermediates of the mTOR signaling network and the basal metabolic pathways are conserved in the fruit fly [11-15].

Regulation of mTORC1 activity by ATP and amino acids depends on a multi-step process that results in the recruitment of an mTORC1 homodimer at the lysosomal membrane in the vicinity of the small GTPase Rheb (Ras homologue enriched in brain) [16-20]. Rheb stimulates mTORC1 activity [21], which in turn regulates several downstream targets. S6Kinase1 (S6K1) is one such kinase, sequentially activated through the phosphorylation of its T389 and T229 residues by mTORC1 and by PDK1 (Phosphoinositide-dependent protein kinase 1), respectively [22, 23]. Further, Rheb activation of mTORC1 is repressed by the tumor suppressor TSC (Tuberous sclerosis complex) that comprises subunits TSC1 and TSC2 [24-27].

The mTORC2 branch resides within the insulin signaling cascade [9]. Binding of insulin or related peptides to their cognate receptors results in recruitment of class I PI3K (Phosphoinositide 3-kinase) to the membrane. PI3K phosphorylates inositol lipids producing phosphatidylinositol-3,4,5-triphosphate (PIP3) [28, 29], while the tumor suppressor PTEN acts as a lipid phosphatase to counteract this process [30]. PIP3 constitutes a membrane docking

site for the protein kinase Akt whose subsequent activation depends on the phosphorylation of its S473 and T308 residues by mTORC2 and PDK1, respectively [31].

Constitutive activation of mTORC1 in MEFs (Mouse embryonic fibroblasts) has been shown to stimulate a metabolic network, including glycolysis, the pentose phosphate pathway and the biosynthesis of fatty acid (FA) and cholesterol [32]. Most of the genes encoding glycolytic enzymes are over-expressed in these cells as are those encoding LDH (lactate dehydrogenase) and Pdk1 (Pyruvate dehydrogenase kinase 1; an inhibitor of mitochondrial pyruvate processing). This suggests that mTORC1-activated MEFs potentiate anaerobic glycolysis and repress the tricarboxylic acid cycle (TCA). Conversely, adipose-specific knockout of raptor to impede mTORC1 formation, results in enhanced uncoupling of mitochondrial activity [33]. The increased lipogenesis observed in mTORC1 stimulated cells depends on a downstream transcriptional regulatory axis involving the cofactor Lipin 1 along with a SREBP (Sterol responsive element binding-protein) family member, which activates genes encoding lipogenic enzymes [32, 34]. Congruently, another study revealed that TSC2 mutant cells become addicted to glucose as a result of mTORC1 hyper-activity [35]. In addition, inhibition of mTORC1 activity revealed that these TSC2 mutant cells become also dependent on glutamine catabolism [36]; mTORC1 potentiates this catabolism to feed TCA anaplerosis, through 1) a S6K/eIF4B/Myc axis that increases glutaminase protein levels [37] and 2) the repression of SIRT4, a mitochondrial sirtuin that inhibits glutamine dehydrogenase [38].

Besides mTORC1 mediated regulation, mTORC2 also impinges on basal metabolism. Intracellular activation of Akt increases ATP levels [39, 40] through the stimulation of GLUT4-mediated glucose uptake [41] and the enhancement of the expression and activity of glycolytic enzymes [42, 43]. Akt also dampens glucose production by suppressing PEPCK (gluconeogenesis), glucose-6-phosphatase (glycogenolyse) and the glycogen synthesis repressor GSK3 [44, 45]. However, in contrast to mTORC1, Akt also promotes mitochondrial metabolism and oxidative phosphorylations [42, 46]. Conversely, hepatic knockout of the mTORC2 specific-subunit rictor results in constitutive gluconeogenesis and impaired glycolysis

112 and lipogenesis [47, 48]. Taken together, these studies strongly emphasize the role of mTOR in
113 metabolic-related diseases and in adjusting metabolism to the nutritional and energetic status
114 [7].

115 In the present study, we investigated the requirement of the glycolytic/lipogenic axis for the
116 cellular growth induced by mTORC1 and mTORC2 hyper-activation in *Drosophila*. As previously
117 demonstrated mTORC1 and mTORC2 reside on independent signaling branches in most
118 *Drosophila* tissues [24, 49-52]. Here, we confirmed mTORC1 and 2 independency in the fat
119 body (FB), the organ that fulfils hepatic and adipose functions to control body homeostasis in
120 *Drosophila* [12, 13, 15]. We analyzed the effect of ubiquitous mTOR activation on glycolysis and
121 lipogenesis. We show that in increase in mTOR activity provokes an apparent enhancement of
122 metabolite consumption. Furthermore, our study reveals that metabolic restriction at the
123 organismal level has dramatic consequences on animal survival, but no effect at the cell-
124 autonomous level, suggesting that within an organism, alternative pathways may operate to
125 compensate local metabolic defects. Nonetheless, at the cell-autonomous level, metabolic
126 restriction can restrain mTORC2- but not mTORC1-induced overgrowth, indicating that the
127 potential compensatory metabolic pathways do not fully operate in the context of mTORC2
128 over-activation.

129

130 **RESULTS**

131 **mTORC1 and mTORC2 independency in the fat body**

132 Previous studies showed that mTORC1 and mTORC2 reside on independent signaling
133 branches in most *Drosophila* tissues [24, 49-52]. Activating either the mTORC1 or the mTORC2
134 signaling branch can be performed by overexpressing Rheb or depleting PTEN, respectively. To
135 investigate mTORC1/2 independency in the FB, we generated somatic clones either over-
136 expressing Rheb (*Rheb*$^{+}$) [53] or homozygote for a *PTEN* mutation (*PTEN*$^{-/-}$) [54]. The
137 precursors of FB cells divide in the embryo; during larval life, the differentiated cells do not

138 divide but endoreplicate their DNA content to reach a giant size [55]. Therefore, to precisely
139 evaluate the effect on cell growth, somatic recombination events were induced during
140 embryogenesis at the stage of proliferation of the FB cell precursors and the resulting MARCM
141 clones were analyzed in the FB of late feeding L3 larvae, prior to the wandering stage that
142 precedes metamorphosis entry. Both *PTEN*$^{-/-}$ and *Rheb*$^{+}$ clonal cells were bigger than the
143 surrounding control cells and this cell size effect was dramatically increased in *PTEN*$^{-/-}$;*Rheb*$^{+}$
144 combined clones (Figure 1A-D and 1M). We next analyzed this growth increase in the context of
145 the previously described *mTOR*$^{2L1}$ and *mTOR*$^{\Delta P}$ mutations. However, we could not find mutant
146 clones in the FB. Consistent with previous studies reporting that mTOR is critically required for
147 cell growth of endoreplicative tissues [54, 56], we reasoned that these clonal cells were likely
148 eliminated by cell competition [57]. Thus, we generated somatic clones in a *Minute* background
149 to slow down the growth of the surrounding control cells. In these conditions, *mTOR* mutant
150 clones could indeed be recovered. Both *mTOR*$^{2L1}$ and *mTOR*$^{\Delta P}$ mutant cells exhibited a
151 dramatic size reduction (Figure 1G and 1J) and this phenotype was dominant in *Rheb*$^{+}$
152 combined clonal cells (compare Figure 1E to 1H and 1K). In contrast, *mTOR*$^{\Delta P}$ but not *mTOR*$^{2L1}$
153 exhibited a clear dominant phenotype over the *PTEN*$^{-/-}$ mutation; the size of *mTOR*$^{\Delta P}$,*PTEN*$^{-/-}$
154 clonal cells was dramatically reduced, whereas *mTOR*$^{2L1}$,*PTEN*$^{-/-}$ clonal cells were giant
155 (compare Figure 1F to 1I and 1L). These findings indicate that the *mTOR*$^{2L1}$ mutation affects
156 mTORC1 but not mTORC2 signaling, whereas *mTOR*$^{\Delta P}$ affects both signaling branches.

157 Next, we used phospho-specific antibodies in immunostaining assays to analyze the
158 phosphorylation of Akt (P-Akt) and of the dS6K target, ribosomal protein rpS6 (P-S6). In *PTEN*$^{-/-}$
159 clonal cells, we observed an increase in the P-Akt intracellular signal (Figure 2A). Importantly
160 the P-Akt intracellular signal was absent in *mTOR*$^{\Delta P}$ cells (Figure 2B) but not affected in
161 *mTOR*$^{2L1}$ cells (Figure 2C). Staining with the rpS6 phospho-specific antibody revealed a patchy
162 signal, with only a subset of cells expressing the P-S6 signal in the FB (Figure 2E-J), a pattern
163 previously described in the wing imaginal disc [58]. Therefore, to evaluate mTORC1 activity, we
164 measured the ratio of P-S6 positive cells among the population of GFP$^{+}$ clonal cells. For control

165 clones, only labeled by GFP, about half of them were P-S6 positive (Figure 2E and 2K),
166 whereas most of the *mTOR*$^{2L1}$ and *mTOR*$^{\Delta P}$ clones were P-S6 negative (Figure 2F, 2G and 2K).
167 Importantly, almost all the *Rheb*$^{+}$ cells were P-S6 positive (Figure 2H and 2K), whereas the ratio
168 of P-S6 positive cells was slightly but not significantly increased in the *PTEN*$^{-/-}$ cell population
169 (Figure 2I and 2K). Taken together, these findings confirm that mTORC1 and mTORC2 operate
170 independently in FB cells and reveal that the *mTOR*$^{2L1}$ mutation affects only mTORC1, whereas
171 the *mTOR*$^{\Delta P}$ mutation affects both signaling branches.

172

173 **Activating mTORC1 or mTORC2 signaling impacts basal metabolism**

174 A number of studies support the notion that mTOR activity controls metabolism to sustain
175 cellular growth. To evaluate how mTORC1 and mTORC2 affect basal metabolism in *Drosophila*,
176 we analyzed various metabolites in whole animals that express the ubiquitous *da-gal4* driver to
177 direct Rheb overexpression (*Rheb*$^{++}$) or PTEN knockdown by RNA interference (*PTEN-RNAi*).
178 Larvae were fed either a standard or a 20%-sucrose supplemented diet (20%-SSD) and 0-5h
179 prepupae were collected, as this is a convenient phase to stage the animals after the feeding
180 period. When fed a standard diet, a high rate of lethality was observed for *Rheb*$^{++}$ and *PTEN-*
181 *RNAi* larvae, although a sufficient number of prepupae could be collected for metabolic analysis.
182 In contrast, none of the *Rheb*$^{++}$ and *PTEN-RNAi* larvae reached the prepupal stage when fed a
183 20%-SSD. Nonetheless, when *Rheb*$^{++}$ and *PTEN-RNAi* larvae were fed a standard diet during
184 early larval life and transferred onto a 20%-SSD at the L2/L3 molting transition, we could
185 recover a few prepupae for metabolic measurements. For both males and females fed a
186 standard diet, the body weight of *Rheb*$^{++}$ and *PTEN-RNAi* prepupae was roughly similar to that
187 of controls (Figure 3A and 3B). Conversely, providing a 20%-SSD resulted in a drop of the
188 prepupal weight of control animals that was significantly compensated in *Rheb*$^{++}$ and *PTEN-*
189 *RNAi* prepupae (Figure 3A and 3B).

190 Next, we measured the total amounts of protein, triacylglycerol (TAG), glycogen and trehalose—
191 the most abundant circulating sugar in *Drosophila*. Although variations in protein levels were

192 observed, none of them were statistically significant (Figure 3C). TAG levels in control prepupae
193 were not affected by sucrose supplementation and did not vary in *PTEN-RNAi*, but were
194 significantly decreased in *Rheb*$^{++}$ animals (Figure 3D). Feeding larvae a 20%-SSD since the
195 L2/L3 molting transition resulted in a marked in increase in glycogen and trehalose levels in
196 control prepupae (Figure 3E-F). In *Rheb*$^{++}$ and, in lower extent, in *PTEN-RNAi* prepupae,
197 glycogen levels were significantly lower than those measured in controls (Figure 3E). Finally,
198 trehalose levels were strongly decreased in both *Rheb*$^{++}$ and *PTEN-RNAi* prepupae fed either a
199 standard or a 20%-SSD as compared to the control (Figure 3F). Taken together, these findings
200 suggest that a ubiquitous increased activity of either mTORC1 or mTORC2 provokes an
201 apparent increase in metabolite consumption. This metabolic rate is correlated with a relative
202 increase in body weight for larvae fed a 20%-SSD, but not for those fed a standard diet. We
203 previously observed that increasing dietary sucrose induced a reduction in food intake [59] that
204 may account for the body weight reduction of control animals. Potentially, food intake could be
205 less affected in *Rheb*$^{++}$ and *PTEN-RNAi* animals, thereby leading to a compensatory effect on
206 body weight. Measuring food intake in *Rheb*$^{++}$ or *PTEN-RNAi* larvae was not applicable since
207 most of them die during larval stage and thus, terminate feeding earlier. In sum, our data
208 indicates that basal metabolism is altered in the few *Rheb*$^{++}$ or *PTEN-RNAi* larvae that survive
209 and further suggests that in most cases stronger metabolic disruption happened, resulting in
210 lethal homeostatic defects.

211

212 **Knocking-down glycolysis at the whole body level**

213 Since manipulating mTOR resulted in a decrease in the levels of TAG and glycogen stores and
214 of circulating trehalose (Figure 3), we asked whether the basal energetic metabolism affected
215 mTOR signaling. First, we ubiquitously expressed interfering RNA against
216 phosphofructokinase1 (*PFK1-RNAi*), pyruvate kinase (*PK-RNAi*) pyruvate dehydrogenase
217 (*PDH-RNAi*) and lactate dehydrogenase (*LDH-RNAi*). PFK1 catalyzes the third glycolytic
218 reaction to form fructose 1,6-bisphophate; PK catalyzes the final glycolytic reaction to form

219 pyruvate; PDH directs the mitochondrial fate of pyruvate, whereas LDH directs its anaerobic fate
220 (Figure 4A). When directed with the ubiquitous *da-gal4* driver, *PK-RNAi* provoked early larval
221 lethality, *PFK1-RNAi* and *PDH-RNAi* provoked larval lethality at L2 or L3 stages, whereas *LDH-*
222 *RNAi* induced a semi-lethal phenotype at larval or pupal stages (Figure 4B).

223 Second, to monitor mTOR activity following ubiquitous knockdown of glycolysis, the *da-gal4*
224 driver was combined with a ubiquitous thermo-sensitive form of the Gal4 inhibitor, Gal80$^{ts}$ (*tub-*
225 *gal80$^{ts}$*) that blocks Gal4 activity at 21°C but not at 29°C, thereby allowing RNAi expression after
226 temperature shift. Each RNAi was ubiquitously induced at early L1 stage and protein extracts
227 were prepared two days later using late L2 larvae. At this stage the larvae were still viable,
228 although those expressing PK-RNAi did not undergo L2/L3 transition and eventually died
229 (Figure 4B). Western-blotting using these L2 protein extracts revealed that RNAi-knockdown of
230 PFK1, LDH or PDH did not affect Akt or dS6K phosphorylation (Figure 4C). In contrast, PK
231 knockdown strongly decreased dS6K phosphorylation and to a lower extent Akt phosphorylation
232 (Figure 4C). These results indicate that mTORC1 signaling may be affected when knocking
233 down PK, but not when knocking down any other enzyme directly linked to glycolysis.
234 Nonetheless, the lethal phenotype of PK-RNAi larvae occurring at the late L2 stage (Figure 4B)
235 might weaken the larvae, inducing a subsequent effect on mTOR signaling.

236 To evaluate the requirement of glycolysis for adult survival, RNAi-knockdown was induced by
237 temperature shift to 29°C in newly emerged flies and lethality was counted every second day. In
238 both males and females, PK and PFK1 knockdown provoked lethality between 10 to 14 days
239 after temperature shift (Figure 4D). Knockdown of PDH and LDH also induced adult lethality,
240 although not as soon as PK and PFK1 knockdown (Figure 4D). As a comparison, we analyzed
241 FASN knockdown in adults; about a quarter of *FASN-RNAi* flies died between 10 to 14 days,
242 while the others survived nearly as well as control flies (Figure 4D). Taken together, these data
243 indicate that glycolysis is essential for both larval development and adult survival. However,
244 prior to the appearance of the deleterious phenotype, glycolysis knockdown is unlikely to
245 impinge on mTOR signaling.

246

247 **Cell-autonomous requirement of glycolysis for mTORC2- but not mTORC1-dependent**
248 **overgrowth**

249 To investigate the requirement of glycolysis to sustain mTOR-dependent growth at the cell-
250 autonomous level, *PFK1-RNAi*, *PK-RNAi*, *PDH-RNAi* and *LDH-RNAi* were induced in *PTEN*$^{-/-}$ or
251 *Rheb*$^{+}$ clones. Except a moderate effect of *PK-RNAi*, clones expressing interfering RNA against
252 these metabolic enzymes did not significantly affect the growth of FB cells (Figure 5A-D and
253 5M). In combined clones, none of the RNAi affected the growth of *Rheb*$^{+}$ clones (Figure 5E-H
254 and 5M). In contrast, the size of *PTEN*$^{-/-}$ clones was significantly decreased when co-expressing
255 RNA against any of these metabolic enzymes (Figure 5I-M). These findings indicate that both
256 aerobic and anaerobic glycolysis are required to sustain mTORC2-dependent overgrowth at the
257 cell-autonomous level. In contrast, reducing glycolysis does not counteract mTORC1-dependent
258 overgrowth, suggesting the existence of compensatory pathways.

259

260 **Effect of Lipogenesis on mTOR signaling**

261 Since glycolysis and FA synthesis are tightly connected metabolic pathways [59], we
262 investigated whether lipogenesis affects mTOR signaling. FA synthesis is catalyzed by FASN
263 (Figure 4A). The *Drosophila* genome encodes three *FASN* genes, *FASN1* is ubiquitously
264 expressed but not *FASN2* or *FASN3* [60-62]. The deletion of the *FASN1* and *FASN2* tandem
265 (*FASN*$^{\Delta 24\text{-}23}$ deletion, hereafter called *FASN*$^{1\text{-}2}$) results in a lethal phenotype that can be rescued
266 by feeding larvae a lipid-complemented diet (beySD) [59, 62]. We observed that beySD-rescued
267 *FASN*$^{1\text{-}2}$ mutant larvae exhibited a delay in development, as measured by the duration of larval
268 development to metamorphosis entry (Figure 6A). Further, when beySD-rescued *FASN*$^{1\text{-}2}$
269 mutant larvae were transferred at the L2/L3 larval transition onto a 10% sucrose-supplemented-
270 beySD, only a few of them completed the third larval stage and, after an extreme developmental
271 delay, entered metamorphosis (Figure 6A). Delay in development can be due to a default in

272 ecdysone production that results in giant pupae [63] or to impaired mTOR signaling that results
273 in reduced body growth [54, 64]. Measurements of prepupal weight revealed that *FASN*$^{1-2}$
274 mutant prepupae exhibited a severe reduction in body weight, whether or not they were
275 supplemented with sucrose (Figure 6B), suggesting a default in mTOR signaling. Therefore, we
276 analyzed the phosphorylation of the *Drosophila* S6Kinase (dS6K) and Akt in protein extracts of
277 late feeding L3 larvae. Western-blotting revealed that the dS6K protein resolved in several
278 bands in *FASN*$^{1-2}$ extracts, whereas Akt protein was unchanged (Figure 6C). These results
279 suggest that dS6K but not Akt might be degraded in the *FASN*$^{1-2}$ mutant background. In
280 addition, dS6K phosphorylation decreased in *FASN*$^{1-2}$ extracts and became barely detectable
281 when *FASN*$^{1-2}$ larvae were fed a sucrose-supplemented-beySD (Figure 6C). Conversely, the
282 phosphorylation of Akt was unaffected in larvae fed a beySD, although it was slightly decreased
283 in larvae fed a sucrose-supplemented-beySD (Figure 6C). This finding contrasts with our
284 previous observation showing that FB explants of *FASN*$^{1-2}$ mutant larvae were hypersensitive to
285 insulin [59]. However, *FASN*$^{1-2}$ mutants also exhibited a decrease in food intake [59], which
286 might induce a systemic suppression of dS6K phosphorylation, while FB explant were cultured
287 in nutrient media supplemented with insulin. Therefore, to determine whether *FASN* mutation
288 affects mTOR signaling at the cell-autonomous level, we analyzed P-S6 and P-Akt in *FASN*$^{1-2}$
289 mutant clones in the FB. As for control clones, about half of the *FASN*$^{1-2}$ clonal cells were P-S6
290 positive (Figure 2J and 2K). Furthermore, no effect on P-Akt was observed in *FASN*$^{1-2}$ clonal
291 cells (Figure 2D). In summary, these findings reveal that disrupting FA synthesis does not
292 significantly affect mTORC1 and mTORC2 signaling at the cell-autonomous level, although it
293 seems to impinge on mTORC1 signaling when inhibited in the whole animal whether directly or
294 indirectly.

295

296 **Cell-autonomous requirement of FA synthesis for mTORC2- but not mTORC1-dependent**
297 **overgrowth**

298 To determine, whether lipogenesis is required at the cell-autonomous level to sustain mTORC1
299 and/or mTORC2 dependent growth, we analyzed *FASN*$^{1-2}$ clones while enhancing either of the
300 mTOR signaling branch in FB cells. We previously reported [59] that *FASN*$^{1-2}$ clonal cells in the
301 FB were slightly reduced in size and that this effect was dramatically increased in larvae fed a
302 20%-SSD (Supplementary Figure S1 and Figure 7M). Therefore, we generated *PTEN*$^{-/-}$ and
303 *Rheb*$^{+}$ clones combined or not with the *FASN*$^{1-2}$ mutation and analyzed them in the FB of larvae
304 fed either a standard diet or a 20%-SSD. As compared to the standard diet, feeding larvae a
305 20%-SSD had no effect on the size of *Rheb*$^{+}$ clonal cells, but significantly reduced the size of
306 *PTEN*$^{-/-}$ and of *PTEN*$^{-/-}$;*Rheb*$^{+}$ clonal cells (Figure 7A-F and 7M). Further, when combined with
307 the *FASN*$^{1-2}$ mutation, *PTEN*$^{-/-}$ but not *Rheb*$^{+}$ clones were significantly reduced in size (Figure
308 7G-H and 7M). The *FASN*$^{1-2}$ mutation also provoked a severe size reduction of *PTEN*$^{-/-}$,*Rheb*$^{+}$
309 clones (Figure 7I and 7M). Moreover, as compared to the standard diet, feeding larvae a 20%-
310 SSD induced a significant size reduction of *FASN*$^{1-2}$;*Rheb*$^{+}$, *FASN*$^{1-2}$,*PTEN*$^{-/-}$ and *FASN*$^{1-2}$,*PTEN*$^{-}$
311 $^{/-}$;*Rheb*$^{+}$ clonal cells (Figure 7J-L and 7M). Of note, except for the *FASN*$^{1-2}$;*Rheb*$^{+}$ clonal cells in
312 larvae fed a 20%-SSD that exhibited a size roughly identical to that of the surrounding control
313 cells (Figure 7J), the cell size was always bigger than the controls (Figure 7M). These findings
314 indicate that, in larvae fed a standard diet, FA synthesis is at least in part required to sustain
315 over-growth induced by mTORC2, but not mTORC1. They also reveal that additional dietary
316 sucrose is rather detrimental for the growth of cells either deficient for FA synthesis or over-
317 active for mTORC2, suggesting that these cells have a restricted homeostatic ability to adjust to
318 an unbalanced diet, whereas mTORC1 activated cells at least in part maintain this ability.

319

320 **DISCUSSION**

321 In this study, we used the powerful *Drosophila* genetics to investigate the functional links
322 between mTOR-dependent growth and the glycolytic/lipogenic axis. On one hand, we
323 dampened this metabolic axis or enhanced mTORC1/2 activity in the whole organism to mimic
324 the effect that might be induced by drug treatment with a systemic inhibitor. On the other hand,

325 to monitor the cell growth process that spans the entire developmental program at the cell-
326 autonomous level, we analyzed clonal FB cells in mosaic animals. Intriguingly, our study reveals
327 apparent contradictory effects between perturbations at the whole body and cell-autonomous
328 levels.

329 At the organismal level, knockdown of glycolytic enzymes or deficiency of FASN result in animal
330 lethality. However, *FASN*$^{1-2}$ mutant animals supplemented with dietary lipids can survive but
331 exhibit a dramatic overall growth suppression. This growth defect might result from a decrease
332 in mTORC1 activity that is strongly reduced in *FASN*$^{1-2}$ mutant animals, suggesting that
333 mTORC1 but not mTORC2 signaling relies on lipogenesis. In contrast, at the cell autonomous
334 level, the mutation of *FASN*$^{1-2}$ restrains mTORC2 but not mTORC1 dependent overgrowth in FB
335 cells. These apparent contradictory findings, suggest that the growth defect and the reduction of
336 mTORC1 activity in *FASN*$^{1-2}$ mutants are not due to the addition of cell-autonomous effects but
337 rather to a systemic regulation. Potentially, FASN default might affect the activity of a specific
338 tissue, as for instance, the neurosecretory cells that synthesize and secrete insulin like peptides,
339 which promote systemic body growth [65]. Alternatively, considering that mTORC1 directly
340 responds to nutrients [18-20], the drop of mTORC1 activity may be a consequence of feeding,
341 since we previously reported a decrease in nutrient uptake in *FASN*$^{1-2}$ mutant animals [59].
342 Consistently, a previous study on the transcription factor mio —the *Drosophila* homologue of
343 mondoA and ChREBP that regulate the glycolytic/lipogenic axis in response to dietary sugar
344 [66, 67]— suggests the existence of a FASN-dependent effect in the FB on the control of food
345 intake [68]. FB-knockdown of *mio* results in the lack of sucrose-induced expression of *FASN1*
346 and in a decrease in food intake. This study suggests that the FASN default perturbs body
347 homeostasis and indirectly affects the neuronal control of feeding behavior. However, it does
348 not exclude that a lipogenic defect in neuronal cells may also directly impinge on feeding
349 behavior. Finally, the drop of mTORC1 activity observed in *FASN*$^{1-2}$ mutants may be a
350 consequence of malonyl-CoA accumulation, since mTOR malonylation has been reported to
351 inhibit mTORC1 but not mTORC2 activity [69]. Malonylation of mTOR may also account for the

352 size reduction of *FASN*$^{1-2}$ mutant cells over-expressing Rheb in animals fed a 20%-SSD,
353 consistent with the increased expression of lipogenic enzymes induced by dietary sucrose [59].
354 Thus, mTOR malonylation and the subsequent decrease in mTORC1 activity might occur only
355 when interfering with a context of high demand for lipogenesis.

356 Our study reveals that over-activation of mTORC1 and to a lesser extent of mTORC2, results in
357 a decrease in glycogen and TAG stores and in circulating trehalose, suggesting that mTOR
358 activation enhances metabolite consumption to sustain cell growth. It is therefore surprising that
359 activation of neither mTORC1 nor mTORC2 induces an increase in body weight. Nonetheless,
360 overall body growth depends on an intricate regulatory network that integrates cell-autonomous
361 effects and humoral messages. For instance, previous studies reported that mTOR activation
362 within the ring gland, results in a systemic decrease in body growth [70-72]. Therefore, mTOR
363 ubiquitous activation is likely to promote the growth of most cells but might concurrently perturb
364 endocrine signals dampening overall growth. Of note, we observed that larvae fed a 20%-SSD
365 result in pupae with reduced body weight, an effect that is partially suppressed when either of
366 the mTORC-signaling branch is over-activated. The fact that the overall body weight of mTOR-
367 stimulated animals is maintained within a range likely compatible with organismal survival
368 contrasts with the observed high rate of lethality. The decrease in stores and circulating sugars
369 suggests that in these animals each cell tends to increase its basal metabolism evoking an
370 egoist behavior that might perturb the equilibrium between cell-autonomous and systemic
371 regulation. Thus, in a stressful situation, as when animals are fed a 20%-SSD, the need of a
372 tight adjustment to an unbalanced diet may enhance the distortion between cell-autonomous
373 effects and systemic regulation, resulting in an increased rate of lethality.

374 In agreement with other studies [24, 49-52], we show that the mTORC1 and mTORC2 branches
375 work independently in the *Drosophila* FB and we provide evidence that the previously described
376 *mTOR*$^{2L1}$ mutation [54] affects mTORC1 signaling only. A plethora of studies in mammalian
377 cells indicate that mTOR activation directs metabolism towards glucose consumption, storage
378 and anabolism [32, 34, 35, 39, 41-43, 73]. Our study rather suggests that in the *Drosophila*

379 larvae, mTOR promotes metabolite consumption through glycolysis but not storage. However,
380 at the cell-autonomous level, we observe that inhibition of lipogenesis or glycolysis restrains
381 neither larval FB cell growth nor overgrowth induced by mTORC1 stimulation in these cells.
382 These findings counteract the idea that mTORC1 potentiates a glycolytic/lipogenic axis [32] to
383 sustain cell growth. To overcome the lack of glycolytic products and of membrane lipids, these
384 cells may benefit of a transfer from neighboring cells and might favor alternative metabolic
385 pathways, including glutamine catabolism to feed TCA anaplerosis which has been shown to be
386 a crucial pathway in mTORC1-stimulated mammalian cells [36-38]. Nonetheless, such
387 compensatory processes do not fully operate to sustain mTORC2-dependent overgrowth. In
388 these cells, the mutation of PTEN results in mTORC2 hyper-activation and potentially impedes
389 the ability to modulate this signaling branch. Therefore, it is tempting to speculate that the
390 modulation of mTORC2 signaling at least in part contributes to the regulation of these
391 compensatory processes.

392 As a coordinator of growth and metabolism, mTOR plays a central role in tumor development [7,
393 74, 75]. PTEN, the tumor suppressor that counteracts PI3K activity upstream of mTORC2
394 signaling, is deficient in several human cancers [30]. Mutation of TSC1 or TSC2, the essential
395 subunits of the tuberous sclerosis complex, is associated with benign tumors but also with brain,
396 kidney and lung destructive diseases [76]. To investigate the role of mTOR regarding tumor
397 development, a recent study reported the generation of liver-specific double knockout mice for
398 TSC1 and PTEN [77]. These mice develop hepatic steatosis that eventually progresses to
399 hepatocellular carcinoma. Both processes are suppressed in mice fed the mTORC1/2 inhibitors
400 INK128, but not the mTORC1 inhibitor rapamycin, supporting an mTORC2 specific effect. The
401 combination of inhibitors against mTOR and metabolism is currently under clinical investigation
402 to fight cancers [7]. Importantly, our study reveals that ubiquitous inhibition of basal metabolism
403 produces dramatic effects during development, while it only moderates cell growth induced by
404 mTOR over-activation. Therefore, the use of drug therapy to fight cancer must be taken with

405 caution, in particular if development is not complete and most efforts should be made to
406 selectively target sick tissues.

407

408 **MATERIAL & METHODS**

409 **Genetics and fly handling**

410 Fly strains: *P[w[+mC]=tubP-GAL80]LL10,P[ry[+t7.2]=neoFRT]40A*, *daughterless(da)-gal4*, *tub-*
411 *gal80$^{ts}$*, *UAS-Dcr-2* (Bloomington Stock Center); *FASN$^{1-2}$* [59]; *mTOR$^{\Delta P}$* [56]; *mTOR$^{2L1}$* and
412 *PTEN* [54]; *EP(UAS)-Rheb* [53]; ); inducible RNA-interfering (*UAS-RNAi*) lines to *PTEN* (NIG
413 5671R-2), *FASN1* (VDRC 29349), *PFK1* (VDRC 3017), *PK* (VDRC 49533) *PDH* (VDRC 40410),
414 *LDH* (VDRC 31192) [78]. The *Minute* stock used was previously referred to as *FRT40/P(arm-*
415 *LacZ w$^{+}$)* [79] but exhibit both developmental delay and short and slender bristles, typically
416 reported as *Minute* phenotype [57]. To generate MARCM clones in the *Minute* background,
417 these flies were recombined with the *P[w[+mC]=tubP-GAL80]LL10,P[ry[+t7.2]=neoFRT]40A*
418 chromosome.

419 The standard media used in this study contained agar (1g), polenta (6g) and yeast (4g) for
420 100ml. Lipid- (beySD) and sugar-complemented media were prepared as previously described
421 [59].

422 To select *FASN$^{1-2}$* mutant larvae, we used a GFP-labelled CyO balancer chromosome. Flies
423 were let to lay eggs on grape juice plates for less than 24 hrs. Then, some beySD media was
424 put in the middle of the plates; larvae that do not express GFP were collected the next day and
425 transferred to fresh tubes. Prepupae were collected once a day to evaluate developmental delay
426 and to measure body weight.

427

428 **Molecular biology and Biochemistry**

429 To test RNAi-knockdown efficacy to the glycolytic enzymes (Supplementary Figure S2), *UAS-*
430 *Dcr-2;da-gal4,tub-gal80$^{ts}$* virgin females were mated with UAS-RNAi males. Flies were let to lay

431 eggs overnight and tubes were kept at 19°C for two days. Tubes were then transferred at 29°C
432 and two days later, larvae of roughly the same size were collected. Reverse transcription and
433 quantitative PCR were performed as previously described [60].

434 Protein extracts for western-blotting were prepared as previously described [51]. Antibody used
435 in for western-blotting have been previously described [51] or commercially provided for Akt
436 (Cell signaling 4054).

437 For metabolic measurements, parental flies were let to lay eggs in tubes for less than 24 hrs at
438 25°C. Tubes were then transferred at 29°C to strengthen the gal4/UAS effect, and using a *UAS-*
439 *Dcr-2* to strengthen the RNAi effect. Larvae were either maintained in the same tubes or
440 selected prior to L2/L3 transition and transferred on 20%-SSD. Collection of prepupae and
441 metabolic measurements were performed as previously described [59].

442

443 **Clonal analysis**

444 All the clones were generated using the MARCM strategy [80]. Parental flies were let to lay
445 eggs at 25°C for seven hrs. Tubes were then heat shocked for 65 minutes in a water bath at
446 38°C so that recombination happens while FB precursor cells are in dividing process. FB from
447 feeding larvae at the end of the L3 stage where dissected, fixed, membranes were labelled with
448 phalloidin and nuclei with DAPI, and FB were mounted as previously described [59]. Image
449 acquisitions were obtained using a Leica SP8 confocal laser-scanning microscope. For immuno
450 staining the phospho-S6 antibody has been previously described [58] and the phospho-Akt
451 commercially provided (Cell signaling 4054). The cell size calculation have been performed as
452 previously described [59] and correspond to a set of experiments that spanned a two-year
453 period. It represent too many replicates, so that it was not possible to make them at the same
454 time. Therefore, for the graphs of cell size measurement (Figure 2M, 5M and 6G), values are
455 reused when they correspond to the same genotype and conditions. This allows a direct
456 comparison between the experiments.

457

458 **Statistical analysis**

459 Statistical analyses were performed with R version 3.4.4, scripts are available on request.
460 Significance for the statistical tests was coded in the following way based on the p-values: ***: 0
461 < p < 0.001; **: 0.001 < p < 0.01; *: 0.01 < p < 0.05. P-values were corrected for multiple testing
462 by a Holm-Bonferroni method [81]. Clone sizes were analyzed with a mixed-effect linear model
463 on the logarithm of cell area, considering the treatment (Genotype and Sucrose conditions) as a
464 fixed effect and Series/Larva as random effects (Figures 1, 5, and 7, Supplementary Table S1).
465 The reported effects (and the corresponding P-values) were obtained from the difference
466 between the (log) area of marked clonal cells and that of control surrounding cells from the
467 same treatment, by setting the appropriate contrast with the "multcomp" package [82], according
468 to the pattern: EA,B = log(MA) – log(WA) – [log(MB) – log(WB)], where EA,B is the difference
469 between treatments (genotype and sucrose levels) A and B, MA and MB standing for the area
470 of marked cells, and WA, WB for the area of control cells in those treatments. This is equivalent
471 to testing whether marked/control cell area ratios differ between treatments. PS6+ clone
472 frequencies were treated as binomial measurements in a mixed-effect generalized linear model
473 "lme4" package [83], featuring Genotype as a fixed effect, and Series/Larva as random effects.
474 Both datasets of pupal weights were analyzed independently with linear models including Sex,
475 Genotype, and Sucrose level effects and all their interaction terms (Figure 3A-B and
476 Supplementary Table S3 for PTEN knockdown and Rheb overexpression; and Figure 6B and
477 Supplementary Table S4 for *FASN*$^{1-2}$ mutants). TAG, Protein, Glycogen, and Threalose
478 concentrations were also analyzed with linear models involving Genotype, Sucrose level, and
479 their interactions as fixed effects (Fig3 and Supplementary Table S3).

480

481 **AKNOWLEDGMENTS**

482 We wish to thank D Petit for preparing the fly media, H Stocker for fly stocks, A Teleman for the
483 phospho-S6 antibody, M Gettings for editing the manuscript, and the NIG and VDRC stock
484 centers for RNAi fly strains.

485

486 **REFERENCES**

487 1. Laplante M, Sabatini DM. mTOR signaling in growth control and disease. Cell.
488 2012;149(2):274-93. PubMed PMID: 22500797.
489 2. Howell JJ, Ricoult SJ, Ben-Sahra I, Manning BD. A growing role for mTOR in promoting
490 anabolic metabolism. Biochem Soc Trans. 2013;41(4):906-12. PubMed PMID: 23863154.
491 3. Lamming DW, Sabatini DM. A Central role for mTOR in lipid homeostasis. Cell Metab.
492 2013;18(4):465-9. PubMed PMID: 23973332.
493 4. Caron A, Richard D, Laplante M. The Roles of mTOR Complexes in Lipid Metabolism.
494 Annu Rev Nutr. 2015;35:321-48. PubMed PMID: 26185979.
495 5. Shimobayashi M, Hall MN. Making new contacts: the mTOR network in metabolism and
496 signalling crosstalk. Nat Rev Mol Cell Biol. 2014;15(3):155-62. PubMed PMID: 24556838.
497 6. Saxton RA, Sabatini DM. mTOR Signaling in Growth, Metabolism, and Disease. Cell.
498 2017;168(6):960-76. doi: 10.1016/j.cell.2017.02.004. PubMed PMID: 28283069; PubMed
499 Central PMCID: PMCPMC5394987.
500 7. Mossmann D, Park S, Hall MN. mTOR signalling and cellular metabolism are mutual
501 determinants in cancer. Nat Rev Cancer. 2018;18(12):744-57. Epub 2018/11/15. doi:
502 10.1038/s41568-018-0074-8. PubMed PMID: 30425336.
503 8. Kim DH, Sarbassov DD, Ali SM, King JE, Latek RR, Erdjument-Bromage H, et al. mTOR
504 interacts with raptor to form a nutrient-sensitive complex that signals to the cell growth
505 machinery. Cell. 2002;110(2):163-75. PubMed PMID: 12150925.
506 9. Sarbassov DD, Guertin DA, Ali SM, Sabatini DM. Phosphorylation and regulation of
507 Akt/PKB by the rictor-mTOR complex. Science. 2005;307(5712):1098-101. PubMed PMID:
508 15718470.

509 10. Ugur B, Chen K, Bellen HJ. Drosophila tools and assays for the study of human diseases.
510 Dis Model Mech. 2016;9(3):235-44. doi: 10.1242/dmm.023762. PubMed PMID: 26935102;
511 PubMed Central PMCID: PMCPMC4833332.
512 11. Montagne J, Radimerski T, Thomas G. Insulin signaling: lessons from the Drosophila
513 tuberous sclerosis complex, a tumor suppressor. Sci STKE. 2001;2001(105):PE36.
514 PubMed PMID: 11675514.
515 12. Padmanabha D, Baker KD. Drosophila gains traction as a repurposed tool to investigate
516 metabolism. Trends Endocrinol Metab. 2014;25(10):518-27. doi:
517 10.1016/j.tem.2014.03.011. PubMed PMID: 24768030.
518 13. Antikainen H, Driscoll M, Haspel G, Dobrowolski R. TOR-mediated regulation of
519 metabolism in aging. Aging Cell. 2017;16(6):1219-33. doi: 10.1111/acel.12689. PubMed
520 PMID: 28971552; PubMed Central PMCID: PMCPMC5676073.
521 14. Wangler MF, Hu Y, Shulman JM. Drosophila and genome-wide association studies: a
522 review and resource for the functional dissection of human complex traits. Dis Model Mech.
523 2017;10(2):77-88. doi: 10.1242/dmm.027680. PubMed PMID: 28151408; PubMed Central
524 PMCID: PMCPMC5312009.
525 15. Lehmann M. Endocrine and physiological regulation of neutral fat storage in Drosophila.
526 Mol Cell Endocrinol. 2018;461:165-77. doi: 10.1016/j.mce.2017.09.008. PubMed PMID:
527 28893568; PubMed Central PMCID: PMCPMC5756521.
528 16. Ma XM, Blenis J. Molecular mechanisms of mTOR-mediated translational control. Nat Rev
529 Mol Cell Biol. 2009;10(5):307-18. PubMed PMID: 19339977.
530 17. Goberdhan DC, Ogmundsdottir MH, Kazi S, Reynolds B, Visvalingam SM, Wilson C, et al.
531 Amino acid sensing and mTOR regulation: inside or out? Biochem Soc Trans. 2009;37(Pt
532 1):248-52. PubMed PMID: 19143641.
533 18. Groenewoud MJ, Zwartkruis FJ. Rheb and mammalian target of rapamycin in mitochondrial
534 homoeostasis. Open Biol. 2013;3(12):130185. PubMed PMID: 24352740.
535 19. Dibble CC, Manning BD. Signal integration by mTORC1 coordinates nutrient input with
536 biosynthetic output. Nat Cell Biol. 2013;15(6):555-64. PubMed PMID: 23728461.

537 20. Montagne J. A Wacky Bridge to mTORC1 Dimerization. Dev Cell. 2016;36(2):129-30.
538 PubMed PMID: 26812011.
539 21. Yang H, Jiang X, Li B, Yang HJ, Miller M, Yang A, et al. Mechanisms of mTORC1 activation
540 by RHEB and inhibition by PRAS40. Nature. 2017;552(7685):368-73. Epub 2017/12/14.
541 doi: 10.1038/nature25023. PubMed PMID: 29236692; PubMed Central PMCID:
542 PMCPMC5750076.
543 22. Montagne J, Thomas G. S6K integrates nutrient and mitogen signals to control cell growth.
544 . In: Hall M, Raff, M., Thomas, G., editor. Cell growth: control of cell size.
545 ed: Cold Spring Harbor Press; 2004. p. 265-98.
546 23. Magnuson B, Ekim B, Fingar DC. Regulation and function of ribosomal protein S6 kinase
547 (S6K) within mTOR signalling networks. Biochem J. 2012;441(1):1-21. PubMed PMID:
548 22168436.
549 24. Radimerski T, Montagne J, Hemmings-Mieszczak M, Thomas G. Lethality of Drosophila
550 lacking TSC tumor suppressor function rescued by reducing dS6K signaling. Genes Dev.
551 2002;16(20):2627-32. PubMed PMID: 12381661.
552 25. Garami A, Zwartkruis FJ, Nobukuni T, Joaquin M, Roccio M, Stocker H, et al. Insulin
553 activation of Rheb, a mediator of mTOR/S6K/4E-BP signaling, is inhibited by TSC1 and 2.
554 Mol Cell. 2003;11(6):1457-66. PubMed PMID: 12820960.
555 26. Inoki K, Li Y, Xu T, Guan KL. Rheb GTPase is a direct target of TSC2 GAP activity and
556 regulates mTOR signaling. Genes Dev. 2003;17(15):1829-34. doi: 10.1101/gad.1110003.
557 PubMed PMID: 12869586; PubMed Central PMCID: PMCPMC196227.
558 27. Dibble CC, Elis W, Menon S, Qin W, Klekota J, Asara JM, et al. TBC1D7 is a third subunit
559 of the TSC1-TSC2 complex upstream of mTORC1. Mol Cell. 2012;47(4):535-46. doi:
560 10.1016/j.molcel.2012.06.009. PubMed PMID: 22795129; PubMed Central PMCID:
561 PMCPMC3693578.
562 28. Engelman JA, Luo J, Cantley LC. The evolution of phosphatidylinositol 3-kinases as
563 regulators of growth and metabolism. Nat Rev Genet. 2006;7(8):606-19. doi:
564 10.1038/nrg1879. PubMed PMID: 16847462.

565 29. Haeusler RA, McGraw TE, Accili D. Biochemical and cellular properties of insulin receptor
566 signalling. Nat Rev Mol Cell Biol. 2018;19(1):31-44. doi: 10.1038/nrm.2017.89. PubMed
567 PMID: 28974775; PubMed Central PMCID: PMCPMC5894887.
568 30. Cully M, You H, Levine AJ, Mak TW. Beyond PTEN mutations: the PI3K pathway as an
569 integrator of multiple inputs during tumorigenesis. Nat Rev Cancer. 2006;6(3):184-92. doi:
570 10.1038/nrc1819. PubMed PMID: 16453012.
571 31. Lien EC, Dibble CC, Toker A. PI3K signaling in cancer: beyond AKT. Curr Opin Cell Biol.
572 2017;45:62-71. doi: 10.1016/j.ceb.2017.02.007. PubMed PMID: 28343126; PubMed Central
573 PMCID: PMCPMC5482768.
574 32. Duvel K, Yecies JL, Menon S, Raman P, Lipovsky AI, Souza AL, et al. Activation of a
575 metabolic gene regulatory network downstream of mTOR complex 1. Mol Cell.
576 2010;39(2):171-83. PubMed PMID: 20670887.
577 33. Polak P, Cybulski N, Feige JN, Auwerx J, Ruegg MA, Hall MN. Adipose-specific knockout
578 of raptor results in lean mice with enhanced mitochondrial respiration. Cell Metab.
579 2008;8(5):399-410. doi: 10.1016/j.cmet.2008.09.003. PubMed PMID: 19046571.
580 34. Peterson TR, Sengupta SS, Harris TE, Carmack AE, Kang SA, Balderas E, et al. mTOR
581 complex 1 regulates lipin 1 localization to control the SREBP pathway. Cell.
582 2011;146(3):408-20. doi: 10.1016/j.cell.2011.06.034. PubMed PMID: 21816276; PubMed
583 Central PMCID: PMCPMC3336367.
584 35. Inoki K, Zhu T, Guan KL. TSC2 mediates cellular energy response to control cell growth
585 and survival. Cell. 2003;115(5):577-90. PubMed PMID: 14651849.
586 36. Choo AY, Kim SG, Vander Heiden MG, Mahoney SJ, Vu H, Yoon SO, et al. Glucose
587 addiction of TSC null cells is caused by failed mTORC1-dependent balancing of metabolic
588 demand with supply. Mol Cell. 2010;38(4):487-99. doi: 10.1016/j.molcel.2010.05.007.
589 PubMed PMID: 20513425; PubMed Central PMCID: PMCPMC2896794.
590 37. Csibi A, Lee G, Yoon SO, Tong H, Ilter D, Elia I, et al. The mTORC1/S6K1 pathway
591 regulates glutamine metabolism through the eIF4B-dependent control of c-Myc translation.

592 Curr Biol. 2014;24(19):2274-80. doi: 10.1016/j.cub.2014.08.007. PubMed PMID: 25220053;
593 PubMed Central PMCID: PMCPMC4190129.
594 38. Csibi A, Fendt SM, Li C, Poulogiannis G, Choo AY, Chapski DJ, et al. The mTORC1
595 pathway stimulates glutamine metabolism and cell proliferation by repressing SIRT4. Cell.
596 2013;153(4):840-54. doi: 10.1016/j.cell.2013.04.023. PubMed PMID: 23663782; PubMed
597 Central PMCID: PMCPMC3684628.
598 39. Hahn-Windgassen A, Nogueira V, Chen CC, Skeen JE, Sonenberg N, Hay N. Akt activates
599 the mammalian target of rapamycin by regulating cellular ATP level and AMPK activity. J
600 Biol Chem. 2005;280(37):32081-9. doi: 10.1074/jbc.M502876200. PubMed PMID:
601 16027121.
602 40. Robey RB, Hay N. Is Akt the "Warburg kinase"?-Akt-energy metabolism interactions and
603 oncogenesis. Semin Cancer Biol. 2009;19(1):25-31. doi: 10.1016/j.semcancer.2008.11.010.
604 PubMed PMID: 19130886; PubMed Central PMCID: PMCPMC2814453.
605 41. Jaldin-Fincati JR, Pavarotti M, Frendo-Cumbo S, Bilan PJ, Klip A. Update on GLUT4
606 Vesicle Traffic: A Cornerstone of Insulin Action. Trends Endocrinol Metab. 2017;28(8):597-
607 611. doi: 10.1016/j.tem.2017.05.002. PubMed PMID: 28602209.
608 42. Gottlob K, Majewski N, Kennedy S, Kandel E, Robey RB, Hay N. Inhibition of early
609 apoptotic events by Akt/PKB is dependent on the first committed step of glycolysis and
610 mitochondrial hexokinase. Genes Dev. 2001;15(11):1406-18. doi: 10.1101/gad.889901.
611 PubMed PMID: 11390360; PubMed Central PMCID: PMCPMC312709.
612 43. Houddane A, Bultot L, Novellasdemunt L, Johanns M, Gueuning MA, Vertommen D, et al.
613 Role of Akt/PKB and PFKFB isoenzymes in the control of glycolysis, cell proliferation and
614 protein synthesis in mitogen-stimulated thymocytes. Cell Signal. 2017;34:23-37. doi:
615 10.1016/j.cellsig.2017.02.019. PubMed PMID: 28235572.
616 44. Nakae J, Kitamura T, Silver DL, Accili D. The forkhead transcription factor Foxo1 (Fkhr)
617 confers insulin sensitivity onto glucose-6-phosphatase expression. J Clin Invest.
618 2001;108(9):1359-67. doi: 10.1172/JCI12876. PubMed PMID: 11696581; PubMed Central
619 PMCID: PMCPMC209440.

620 45. McManus EJ, Sakamoto K, Armit LJ, Ronaldson L, Shpiro N, Marquez R, et al. Role that
621 phosphorylation of GSK3 plays in insulin and Wnt signalling defined by knockin analysis.
622 EMBO J. 2005;24(8):1571-83. doi: 10.1038/sj.emboj.7600633. PubMed PMID: 15791206;
623 PubMed Central PMCID: PMCPMC1142569.
624 46. Majewski N, Nogueira V, Bhaskar P, Coy PE, Skeen JE, Gottlob K, et al. Hexokinase-
625 mitochondria interaction mediated by Akt is required to inhibit apoptosis in the presence or
626 absence of Bax and Bak. Mol Cell. 2004;16(5):819-30. doi: 10.1016/j.molcel.2004.11.014.
627 PubMed PMID: 15574336.
628 47. Hagiwara A, Cornu M, Cybulski N, Polak P, Betz C, Trapani F, et al. Hepatic mTORC2
629 activates glycolysis and lipogenesis through Akt, glucokinase, and SREBP1c. Cell Metab.
630 2012;15(5):725-38. doi: 10.1016/j.cmet.2012.03.015. PubMed PMID: 22521878.
631 48. Yuan M, Pino E, Wu L, Kacergis M, Soukas AA. Identification of Akt-independent regulation
632 of hepatic lipogenesis by mammalian target of rapamycin (mTOR) complex 2. J Biol Chem.
633 2012;287(35):29579-88. doi: 10.1074/jbc.M112.386854. PubMed PMID: 22773877;
634 PubMed Central PMCID: PMCPMC3436168.
635 49. Radimerski T, Montagne J, Rintelen F, Stocker H, van der Kaay J, Downes CP, et al. dS6K-
636 regulated cell growth is dPKB/dPI(3)K-independent, but requires dPDK1. Nat Cell Biol.
637 2002;4(3):251-5. PubMed PMID: 11862217.
638 50. Dong J, Pan D. Tsc2 is not a critical target of Akt during normal Drosophila development.
639 Genes Dev. 2004;18(20):2479-84. PubMed PMID: 15466161.
640 51. Montagne J, Lecerf C, Parvy JP, Bennion JM, Radimerski T, Ruhf ML, et al. The nuclear
641 receptor DHR3 modulates dS6 kinase-dependent growth in Drosophila. PLoS Genet.
642 2010;6:e1000937. PubMed PMID: 20463884.
643 52. Pallares-Cartes C, Cakan-Akdogan G, Teleman AA. Tissue-specific coupling between
644 insulin/IGF and TORC1 signaling via PRAS40 in Drosophila. Dev Cell. 2012;22(1):172-82.
645 doi: 10.1016/j.devcel.2011.10.029. PubMed PMID: 22264732.

646 53. Stocker H, Radimerski T, Schindelholz B, Wittwer F, Belawat P, Daram P, et al. Rheb is an
647 essential regulator of S6K in controlling cell growth in Drosophila. Nat Cell Biol.
648 2003;5(6):559-65. PubMed PMID: 12766775.
649 54. Oldham S, Montagne J, Radimerski T, Thomas G, Hafen E. Genetic and biochemical
650 characterization of dTOR, the Drosophila homolog of the target of rapamycin. Genes Dev.
651 2000;14(21):2689-94. PubMed PMID: 11069885.
652 55. Edgar BA, Orr-Weaver TL. Endoreplication cell cycles: more for less. Cell.
653 2001;105(3):297-306. PubMed PMID: 11348589.
654 56. Zhang H, Stallock JP, Ng JC, Reinhard C, Neufeld TP. Regulation of cellular growth by the
655 Drosophila target of rapamycin dTOR. Genes Dev. 2000;14(21):2712-24. PubMed PMID:
656 11069888.
657 57. Morata G, Ripoll P. Minutes: mutants of drosophila autonomously affecting cell division rate.
658 Dev Biol. 1975;42(2):211-21. PubMed PMID: 1116643.
659 58. Romero-Pozuelo J, Demetriades C, Schroeder P, Teleman AA. CycD/Cdk4 and
660 Discontinuities in Dpp Signaling Activate TORC1 in the Drosophila Wing Disc. Dev Cell.
661 2017;42(4):376-87 e5. doi: 10.1016/j.devcel.2017.07.019. PubMed PMID: 28829945.
662 59. Garrido D, Rubin T, Poidevin M, Maroni B, Le Rouzic A, Parvy JP, et al. Fatty Acid
663 Synthase Cooperates with Glyoxalase 1 to Protect against Sugar Toxicity. PLoS Genet.
664 2015;11(2):e1004995. PubMed PMID: 25692475.
665 60. Parvy JP, Napal L, Rubin T, Poidevin M, Perrin L, Wicker-Thomas C, et al. Drosophila
666 melanogaster Acetyl-CoA-carboxylase sustains a fatty acid-dependent remote signal to
667 waterproof the respiratory system. PLoS Genet. 2012;8(8):e1002925. PubMed PMID:
668 22956916.
669 61. Chung H, Loehlin DW, Dufour HD, Vaccarro K, Millar JG, Carroll SB. A single gene affects
670 both ecological divergence and mate choice in Drosophila. Science. 2014;343(6175):1148-
671 51. PubMed PMID: 24526311.

672 62. Wicker-Thomas C, Garrido D, Bontonou G, Napal L, Mazuras N, Denis B, et al. Flexible
673 origin of hydrocarbon/pheromone precursors in Drosophila melanogaster. J Lipid Res.
674 2015;56(11):2094-101. PubMed PMID: 26353752.
675 63. Parvy JP, Wang P, Garrido D, Maria A, Blais C, Poidevin M, et al. Forward and feedback
676 regulation of cyclic steroid production in Drosophila melanogaster. Development.
677 2014;141(20):3955-65. PubMed PMID: 25252945.
678 64. Montagne J, Stewart MJ, Stocker H, Hafen E, Kozma SC, Thomas G. Drosophila S6
679 kinase: a regulator of cell size. Science. 1999;285(5436):2126-9. PubMed PMID:
680 10497130.
681 65. Rulifson EJ, Kim SK, Nusse R. Ablation of insulin-producing neurons in flies: growth and
682 diabetic phenotypes. Science. 2002;296(5570):1118-20. PubMed PMID: 12004130.
683 66. Mattila J, Havula E, Suominen E, Teesalu M, Surakka I, Hynynen R, et al. Mondo-Mlx
684 Mediates Organismal Sugar Sensing through the Gli-Similar Transcription Factor
685 Sugarbabe. Cell Rep. 2015;13(2):350-64. PubMed PMID: 26440885.
686 67. Richards P, Ourabah S, Montagne J, Burnol AF, Postic C, Guilmeau S. MondoA/ChREBP:
687 The usual suspects of transcriptional glucose sensing; Implication in pathophysiology.
688 Metabolism. 2017;70:133-51. doi: 10.1016/j.metabol.2017.01.033. PubMed PMID:
689 28403938.
690 68. Sassu ED, McDermott JE, Keys BJ, Esmaeili M, Keene AC, Birnbaum MJ, et al.
691 Mio/dChREBP coordinately increases fat mass by regulating lipid synthesis and feeding
692 behavior in Drosophila. Biochem Biophys Res Commun. 2012;426(1):43-8. doi:
693 10.1016/j.bbrc.2012.08.028. PubMed PMID: 22910416; PubMed Central PMCID:
694 PMCPMC3445662.
695 69. Bruning U, Morales-Rodriguez F, Kalucka J, Goveia J, Taverna F, Queiroz KCS, et al.
696 Impairment of Angiogenesis by Fatty Acid Synthase Inhibition Involves mTOR Malonylation.
697 Cell Metab. 2018;28(6):866-80 e15. Epub 2018/08/28. doi: 10.1016/j.cmet.2018.07.019.
698 PubMed PMID: 30146486.

699 70. Caldwell PE, Walkiewicz M, Stern M. Ras activity in the Drosophila prothoracic gland
700 regulates body size and developmental rate via ecdysone release. Curr Biol.
701 2005;15(20):1785-95. PubMed PMID: 16182526.
702 71. Colombani J, Bianchini L, Layalle S, Pondeville E, Dauphin-Villemant C, Antoniewski C, et
703 al. Antagonistic actions of ecdysone and insulins determine final size in Drosophila.
704 Science. 2005;310(5748):667-70. PubMed PMID: 16179433.
705 72. Mirth C. Ecdysteroid control of metamorphosis in the differentiating adult leg structures of
706 Drosophila melanogaster. Dev Biol. 2005;278(1):163-74. PubMed PMID: 15649469.
707 73. Wipperman MF, Montrose DC, Gotto AM, Jr., Hajjar DP. Mammalian Target of Rapamycin:
708 A Metabolic Rheostat for Regulating Adipose Tissue Function and Cardiovascular Health.
709 Am J Pathol. 2019;189(3):492-501. Epub 2019/02/26. doi: 10.1016/j.ajpath.2018.11.013.
710 PubMed PMID: 30803496.
711 74. Harachi M, Masui K, Okamura Y, Tsukui R, Mischel PS, Shibata N. mTOR Complexes as a
712 Nutrient Sensor for Driving Cancer Progression. Int J Mol Sci. 2018;19(10). Epub
713 2018/10/24. doi: 10.3390/ijms19103267. PubMed PMID: 30347859.
714 75. Tian T, Li X, Zhang J. mTOR Signaling in Cancer and mTOR Inhibitors in Solid Tumor
715 Targeting Therapy. Int J Mol Sci. 2019;20(3). Epub 2019/02/14. doi: 10.3390/ijms20030755.
716 PubMed PMID: 30754640; PubMed Central PMCID: PMCPMC6387042.
717 76. Henske EP, Jozwiak S, Kingswood JC, Sampson JR, Thiele EA. Tuberous sclerosis
718 complex. Nat Rev Dis Primers. 2016;2:16035. doi: 10.1038/nrdp.2016.35. PubMed PMID:
719 27226234.
720 77. Guri Y, Colombi M, Dazert E, Hindupur SK, Roszik J, Moes S, et al. mTORC2 Promotes
721 Tumorigenesis via Lipid Synthesis. Cancer Cell. 2017;32(6):807-23 e12. doi:
722 10.1016/j.ccell.2017.11.011. PubMed PMID: 29232555.
723 78. Dietzl G, Chen D, Schnorrer F, Su KC, Barinova Y, Fellner M, et al. A genome-wide
724 transgenic RNAi library for conditional gene inactivation in Drosophila. Nature.
725 2007;448(7150):151-6. PubMed PMID: 17625558.

726 79. Bohni R, Riesgo-Escovar J, Oldham S, Brogiolo W, Stocker H, Andruss BF, et al.
727 Autonomous control of cell and organ size by CHICO, a Drosophila homolog of vertebrate
728 IRS1-4. Cell. 1999;97(7):865-75. PubMed PMID: 10399915.
729 80. Lee T, Luo L. Mosaic analysis with a repressible cell marker (MARCM) for Drosophila
730 neural development. Trends Neurosci. 2001;24(5):251-4. PubMed PMID: 11311363.
731 81. Holm S. A simple sequentially rejective multiple test procedure. Scand J Statist. 1079;6(65-
732 70).
733 82. Hothorn T, Bretz F, Westfall P. Simultaneous inference in general parametric models. Biom
734 J. 2008;50(3):346-63. Epub 2008/05/16. doi: 10.1002/bimj.200810425. PubMed PMID:
735 18481363.
736 83. Bates D, Mächler M, Bolker BM, Walker S. Fitting Linear Mixed-Effects Models Using lme4.
737 Journal of Statistical Software. 2015;67(1):1-48. doi: 10.18637/jss.v067.i01.

738

739 **FIGURE LEGENDS**

740 **Figure 1: mTORC1 and mTORC2 dependent growth in FB cells.** (**A-L**) MARCM clones
741 labeled by GFP (green) in the FB of L3 larvae. Nuclei were labeled with DAPI (silver) and
742 membranes with phalloidin (red). Control (A), *Rheb*$^{+}$ (B), *PTEN*$^{-/-}$ (C) and *PTEN*$^{-/-}$;*Rheb*$^{+}$ (D)
743 clones were generated in a wild type background. *Rheb*$^{+}$ (E), *PTEN*$^{-/-}$ (F), *mTOR*$^{2L1}$ (G)
744 *mTOR*$^{2L1}$, *Rheb*$^{+}$ (H) *mTOR*$^{2L1}$,*PTEN*$^{-/-}$ (I), *mTOR*$^{\Delta P}$ (J), *mTOR*$^{\Delta P}$,*Rheb*$^{+}$ (K) and *mTOR*$^{\Delta P}$,*PTEN*$^{-}$
745 $^{/-}$ (L) clones were generated in a *Minute* (*M*) background. Scale bars: 50µm. (**M**) Relative size of
746 control (Co), *Rheb*$^{+}$, *PTEN*$^{-/-}$, and *PTEN*$^{-/-}$;*Rheb*$^{+}$ clonal cells generated in a wild type
747 background.

748

749 **Figure 2: mTORC1 and mTORC2 activity in FB cells.** (**A-J**) MARCM clones labeled by GFP
750 (green) in the FB of L3 larvae. Clones were generated in a wild type (A,D,E,H,I,J) or a *Minute*
751 (B,C,F,G) background and nuclei were labeled with DAPI (silver). FB tissues with *PTEN*$^{-/-}$ (A),

752 *mTOR$^{\Delta P}$* (B), *mTOR$^{2L1}$* (C) and *FASN$^{1-2}$* (J) clones were stained with a phospho-AKT antibody.
753 FB tissues with control (D), *mTOR$^{\Delta P}$* (E), *mTOR$^{2L1}$* (F) *Rheb$^{+}$* (G), *PTEN$^{-/-}$* (H) and *FASN$^{1-2}$* (I)
754 clones were stained with a phospho-S6 antibody. Scale bars: 50µm. (**K**) Percentage of P-S6
755 positive clones with respect to the total number of MARCM clones for control, *FASN$^{1-2}$*, *PTEN$^{-/-}$*,
756 *Rheb$^{+}$*, *mTOR$^{2L1}$* and *mTOR$^{\Delta P}$* genotypes.

757

758 **Figure 3: Enhanced mTORC1 or mTORC2 signaling affects larval metabolism.** (**A-B**) Body
759 weight of female (A) and male (B) prepupae formed from larvae fed either a standard (0%) or a
760 20%-SSD (20%) as from the L2/L3 transition. (**C-F**) Measurement of total protein (C), TAG (D),
761 glycogen (E) and trehalose (F) levels in prepupae fed either a standard or a 20%-SSD.
762 Prepupae used in these measurements were the F1 progeny from *da-gal4* virgin females mated
763 to either control (Co), *EP(UAS)-Rheb* (*Rheb$^{++}$*) or *UAS-PTEN-RNAi* (*PTEN-Ri*) males.

764

765 **Figure 4: Glycolysis knockdown in whole organisms.** (**A**) Scheme of basal metabolism.
766 Glucose and trehalose enter glycolysis as glucose-6P, whereas fructose follows a distinct
767 pathway to triose-P. Enzymes investigated in the present study are marked in red. (**B**)
768 Phenotype of ubiquitous RNAi knockdown of PFK1, PK, LDH and PDH. Flies were left to lay
769 eggs overnight either at 29°C (column 0h) or at 19°C and transferred to 29°C the day after
770 (column 24h); then development proceeded at 29°C (i.e. the temperature that inactivates
771 Gal80). (**C**) Western-blot analysis of total (top) or phosphorylated (mid) dS6K (left) or Akt (right)
772 proteins; tubulin (bottom) was used as a loading control. Protein extracts were prepared with
773 late L2 control larvae (Co) or L2 larvae expressing RNAi against the indicated metabolic
774 enzymes. (**E-F**) Survival at 29°C of male (top) and female (bottom) control flies or flies
775 expressing RNAi against the indicated metabolic enzymes as from adult eclosion.

776

777 **Figure 5: Cell-autonomous requirement of glycolytic enzymes for mTOR-dependent**
778 **overgrowth.** (**A-G**) MARCM clones labeled by GFP (green) in the FB of L3 larvae. Nuclei were
779 labeled with DAPI (silver) and membranes with phalloidin (red). Genotypes of MARCM clones
780 are: *PFK1-RNAi* (A), *PK-RNAi* (B), *LDH-RNAi* (C), *PDH-RNAi* (D), *Rheb*$^{+}$,*PFK1-RNAi* (E),
781 *Rheb*$^{+}$,*PK-RNAi* (F), *Rheb*$^{+}$,*LDH-RNAi* (G), *Rheb*$^{+}$,*PDH-RNAi* (H), *PTEN*$^{-/-}$;*PFK1-RNAi* (I),
782 *PTEN*$^{-/-}$;*PK-RNAi* (J), *PTEN*$^{-/-}$;*PDH-RNAi* (K) and *PTEN*$^{-/-}$;*PDH-RNAi* (L). Scale bars: 50µm. (**M**)
783 Relative size of clonal cells corresponding to the clones shown in A-L, and in Figure 2A for
784 control (Co).

785

786 **Figure 6: *FASN*$^{1-2}$ mutation affects developmental growth and mTOR signaling.** (**A**)
787 Developmental duration from egg laying to metamorphosis onset of *w*$^{1118}$ control (Co) and
788 *FASN*$^{1-2}$ (FASN) larvae fed either a beySD (0%) or a 10% sucrose-supplemented-beySD as
789 from the L2/L3 transition (10%); n: total number of larvae collected for each condition. (**B**)
790 Prepupal weight of females (left) and males (right) as listed in 4A; the numbers of weighted
791 prepupae are indicated above each sample. (**C**) Western-blot analysis of (from top to bottom)
792 total dS6K, phosphorylated dS6K, total Akt, phosphorylated Akt and total tubulin as a loading
793 control. Protein extracts were prepared from feeding L3 larvae prior to the wandering stage as
794 listed in 4A. For each condition, at least 30 larvae were used to prepare protein extracts.

795

796 **Figure 7: Cell-autonomous requirement of FASN activity for mTOR-dependent**
797 **overgrowth.** (**A-L**) MARCM clones labeled by GFP (green) in the FB of L3 larvae fed either a
798 standard (A-C, G-I) or a 20%-SSD (D-E, J-L). Nuclei were labeled with DAPI (silver) and
799 membranes with phalloidin (red). Genotypes of MARCM clones are: *Rheb*$^{+}$ (A,D), *PTEN*$^{-/-}$ (B,E)
800 *PTEN*$^{-/-}$,*Rheb*$^{+}$ (C,F), *FASN*$^{1-2}$;*Rheb*$^{+}$ (G,J) *FASN*$^{1-2}$,*PTEN*$^{-/-}$ (H,K) and the *FASN*$^{1-2}$,*PTEN*$^{-/-}$
801 ;*Rheb*$^{+}$ (I,L). Scale bars: 50µm. (**M**) Relative size of clonal cells corresponding to the clones
802 shown in A-L and in supplementary Fig S1 for *FASN*$^{1-2}$ and Figure 1A for control (Co).

803

804 **SUPPORTING INFORMATIONS**

805 **S1 Table. Statistical tests corresponding to figures 1M (A), 5M (B), and 7M (C).** The model
806 tests for the difference is the log ratio of *GFP*$^{+}$*/GFP*$^{-}$*surrounding* cells between pairs of
807 genotypes (Co = control), accounting for larvae and series random effects (see the Methods
808 section). P-values were corrected for multiple testing (Holm-Bonferroni method) and quantify the
809 risk of rejecting the true null hypothesis at the table level.

810

811 **S2 Table. Statistical test of the difference in frequency between MARCM clones to**
812 **control.** The model is a mixed effect, generalized linear model considering frequencies as
813 binomial data and genotype as a fixed effect, while larvae / series were random effects. P-
814 values were adjusted for multiple testing by a Holm-Bonferroni correction.

815

816 **S3 Table. Statistical tests corresponding to Figure 3.** Differences in male (A) or female (B)
817 weight, in protein (C), in TAG (D), in glycogen (E) and in trehalose (F) between control (Co) and
818 prepupae that ubiquitously express either Rheb (*Rheb*$^{++}$) or an RNAi to PTEN (*PTENi*). The
819 column at the right indicates P-values corrected for multiple testing (Holm-Bonferoni correction).

820

821 **S4 Table. Statistical tests corresponding to Figure 6B.** Prepupal weight differences in males
822 and females (Estimate and standard error, in mg) between control ($w^{-}$) and *FASN*$^{1-2}$ animals fed
823 either a standard (0%) or a sucrose enriched diet (10%). The **Pr** column (right) indicates P-
824 values corrected for multiple testing (Holm-Bonferoni correction).

825

826 **S1 Fig. Effect of dietary sugar on *FASN*$^{1-2}$ mutant cells.** *FASN*$^{1-2}$ MARCM clones labeled by
827 GFP (green) in the FB of L3 larvae fed either a standard (A) or a 20%-SSD (B). Nuclei are
828 labeled with DAPI (silver) and membranes by phalloidin (red). Scale bars: 50μm.

829

830 **S2 Fig. Knockdown efficacy of the RNAi to the glycolytic enzymes.** (**A**) mRNA expression
831 in control larvae (blue bars, +/- standard error) was adjusted to 100. mRNA levels after RNAi
832 knockdown (red bars, +/- standard error) was calculated as a percentage of corresponding
833 expression in control larvae. (**B**) Oligonucleotides used in RT-Q-PCR for each glycolytic
834 enzyme.

835

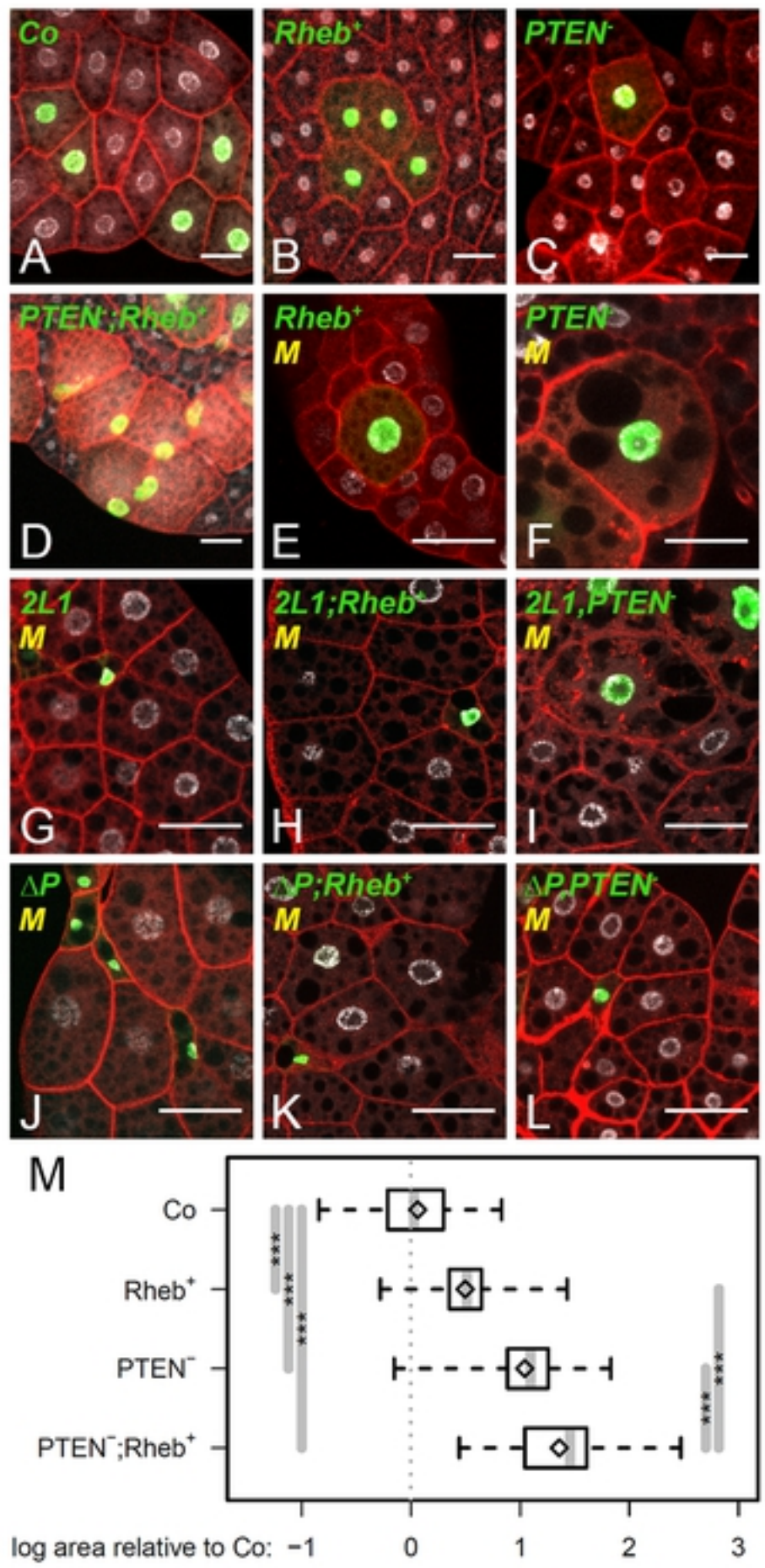
Co
A
Rheb+
B
PTEN-
C
PTEN-;Rheb+
D
Rheb+
M
E
PTEN-
M
F
2L1
M
G
2L1;Rheb+
M
H
2L1,PTEN-
M
I
ΔP
M
J
ΔP;Rheb+
M
K
ΔP,PTEN-
M
L
M
Co
Rheb+
PTEN-
PTEN-;Rheb+
***
***
***
***
***
log area relative to Co: −1
0
1
2
3

Figure 1

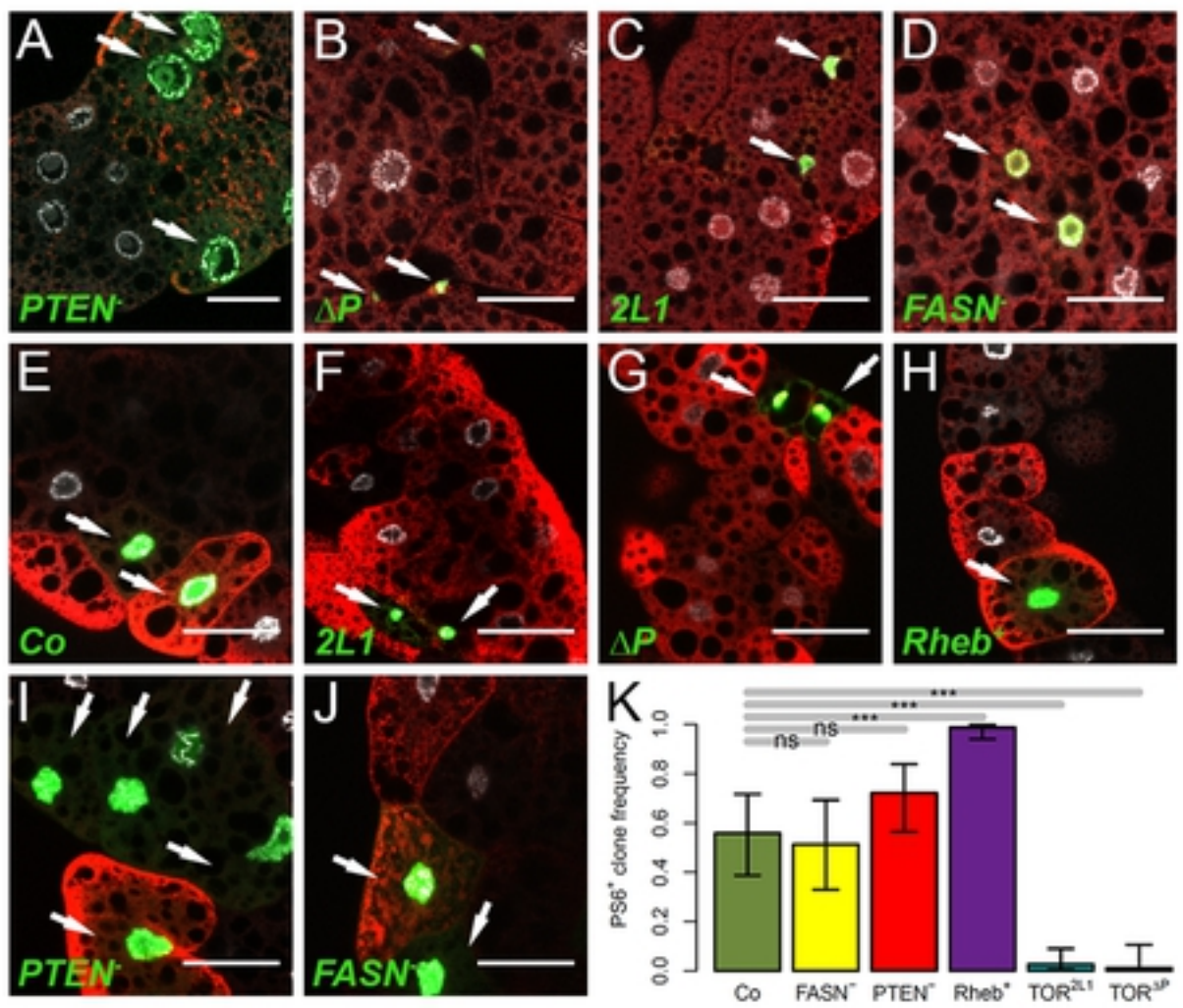
A
PTEN
B
ΔP
C
2L1
D
FASN
E
Co
F
2L1
G
ΔP
H
Rheb
I
PTEN
J
FASN
K
PS6+ clone frequency
0.0
0.2
0.4
0.6
0.8
1.0
ns
ns
***
***
***
Co
FASN
PTEN
Rheb
TOR2L1
TORΔP

Figure 2

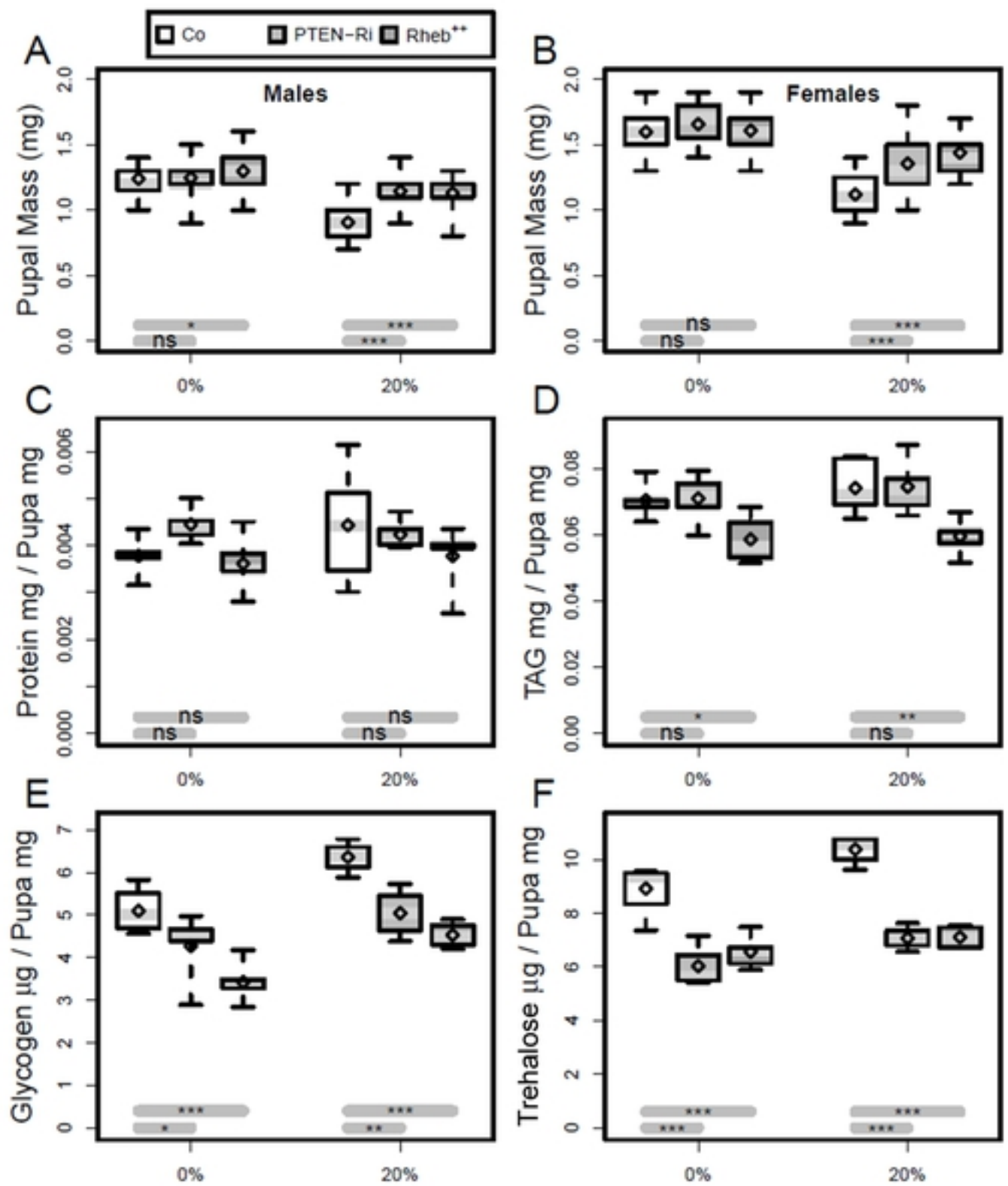
Co
PTEN-Ri
Rheb++
A
Males
Pupal Mass (mg)
B
Females
Pupal Mass (mg)
C
Protein mg / Pupa mg
D
TAG mg / Pupa mg
E
Glycogen µg / Pupa mg
F
Trehalose µg / Pupa mg
0%
20%
ns
*
**
***

Figure 3

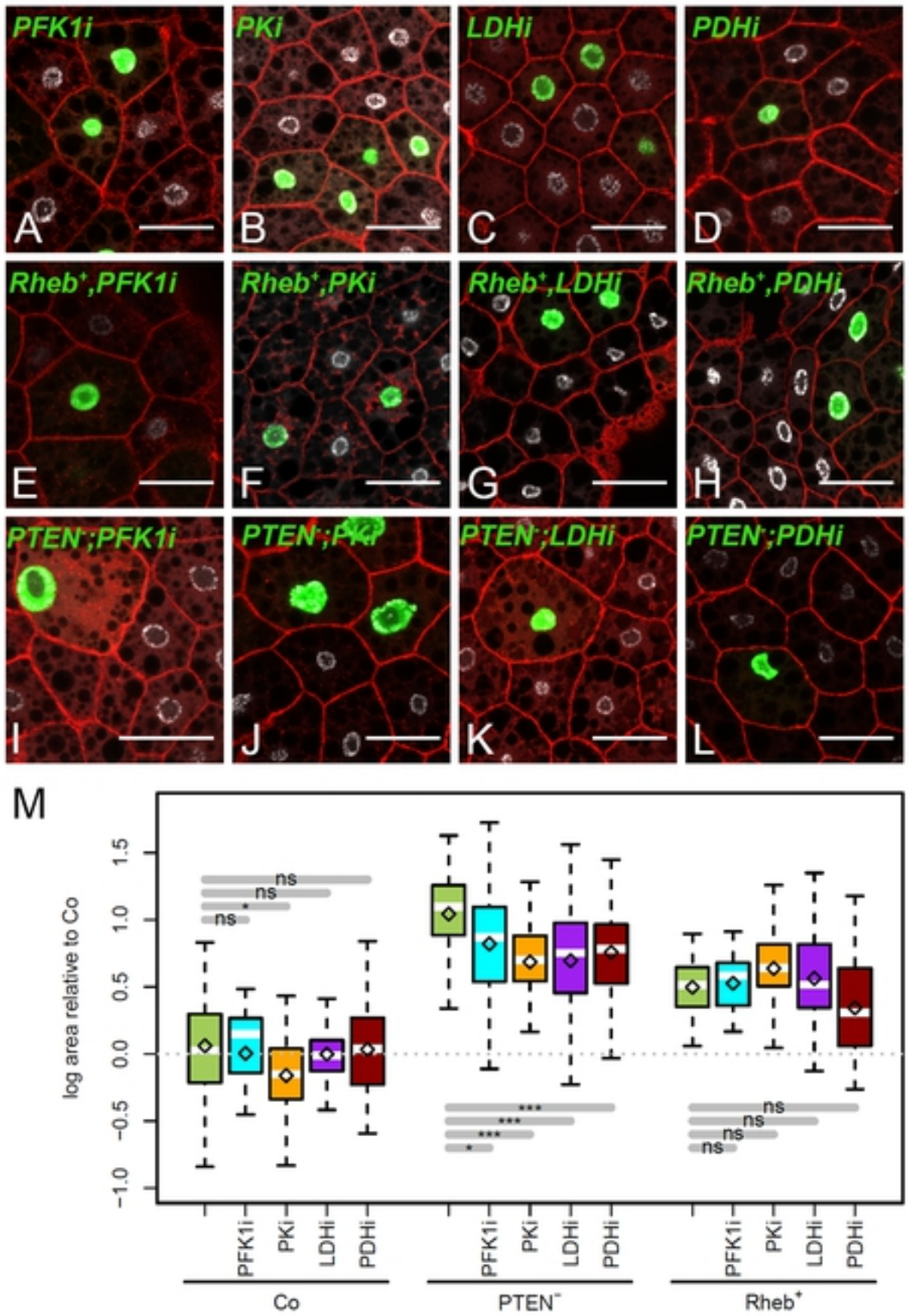
PFK1i
PKi
LDHi
PDHi
A
B
C
D
Rheb+,PFK1i
Rheb+,PKi
Rheb+,LDHi
Rheb+,PDHi
E
F
G
H
PTEN-;PFK1i
PTEN-;PKi
PTEN-;LDHi
PTEN-;PDHi
I
J
K
L
M
log area relative to Co
1.5
1.0
0.5
0.0
−0.5
−1.0
ns
*
***
PFK1i
PKi
LDHi
PDHi
Co
PTEN-
Rheb+

Figure 5

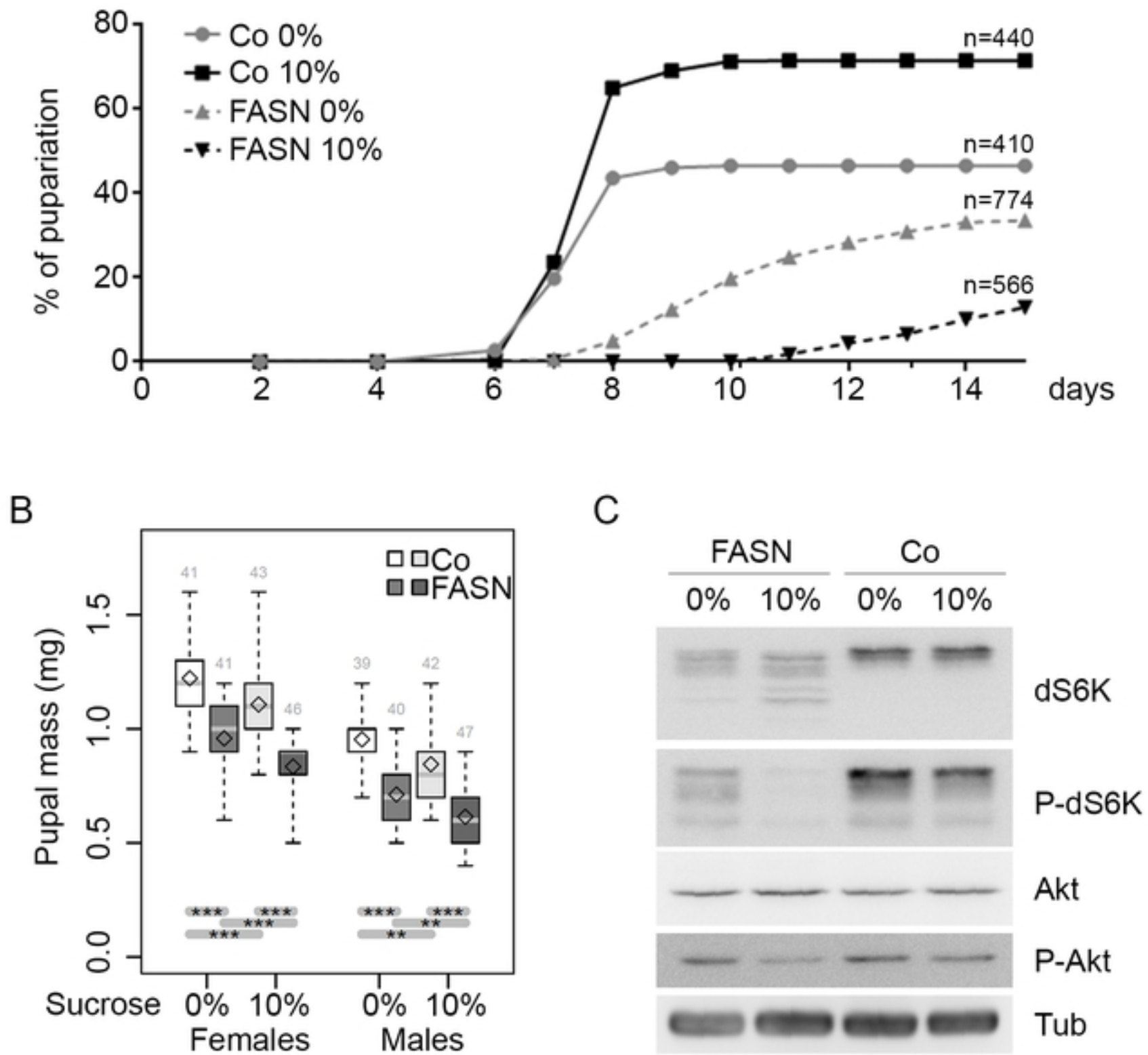
A
Co 0%
Co 10%
FASN 0%
FASN 10%
% of puparation
days
n=440
n=410
n=774
n=566
B
Co
FASN
Pupal mass (mg)
Sucrose
0%
10%
Females
Males
C
FASN
Co
0%
10%
dS6K
P-dS6K
Akt
P-Akt
Tub

Figure 6

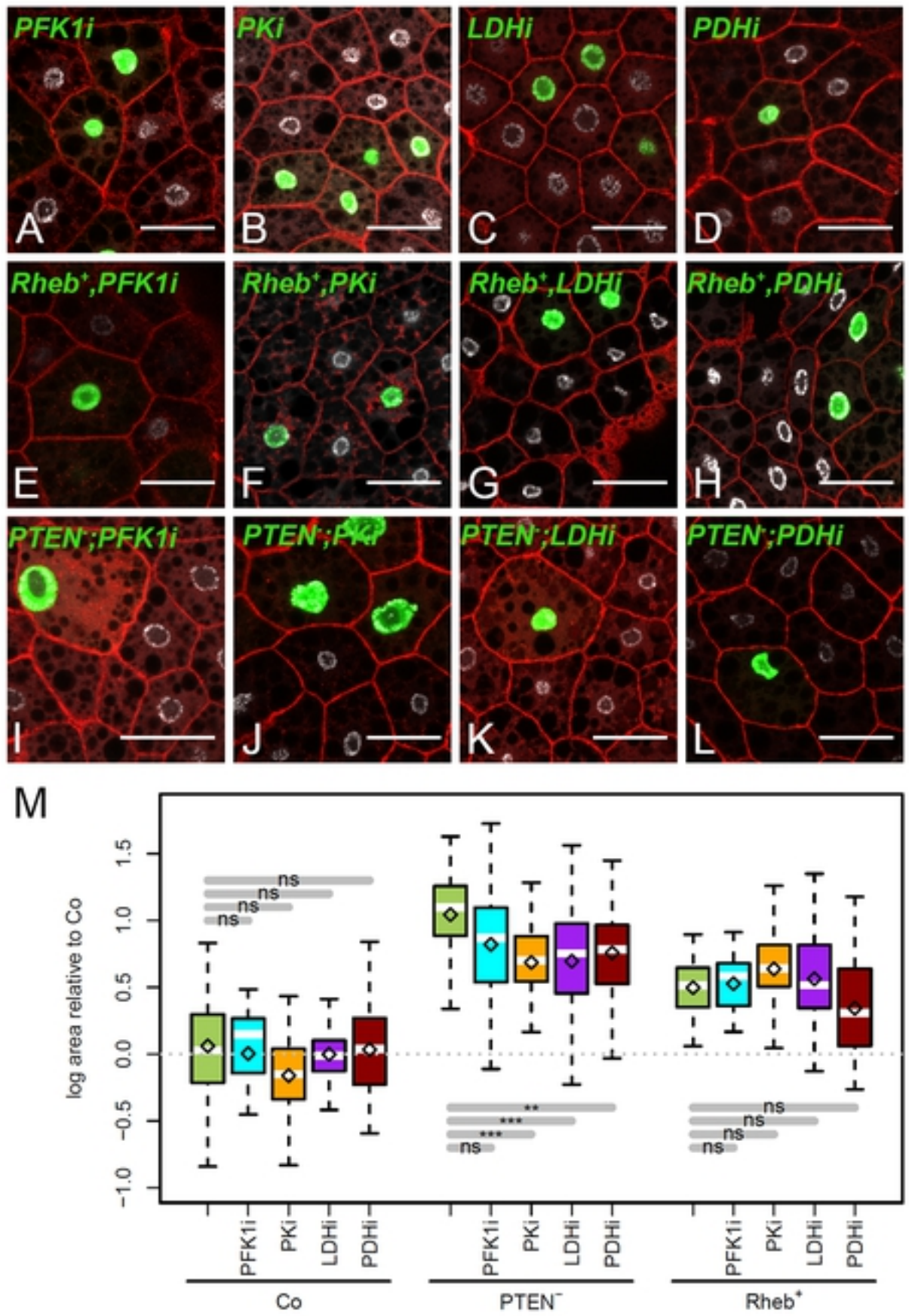
PFK1i
PKi
LDHi
PDHi
A
B
C
D
Rheb+,PFK1i
Rheb+,PKi
Rheb+,LDHi
Rheb+,PDHi
E
F
G
H
PTEN-;PFK1i
PTEN-;PKi
PTEN-;LDHi
PTEN-;PDHi
I
J
K
L
M
log area relative to Co
1.5
1.0
0.5
0.0
−0.5
−1.0
ns
**
***
PFK1i
PKi
LDHi
PDHi
Co
PTEN-
Rheb+

Figure 7

A

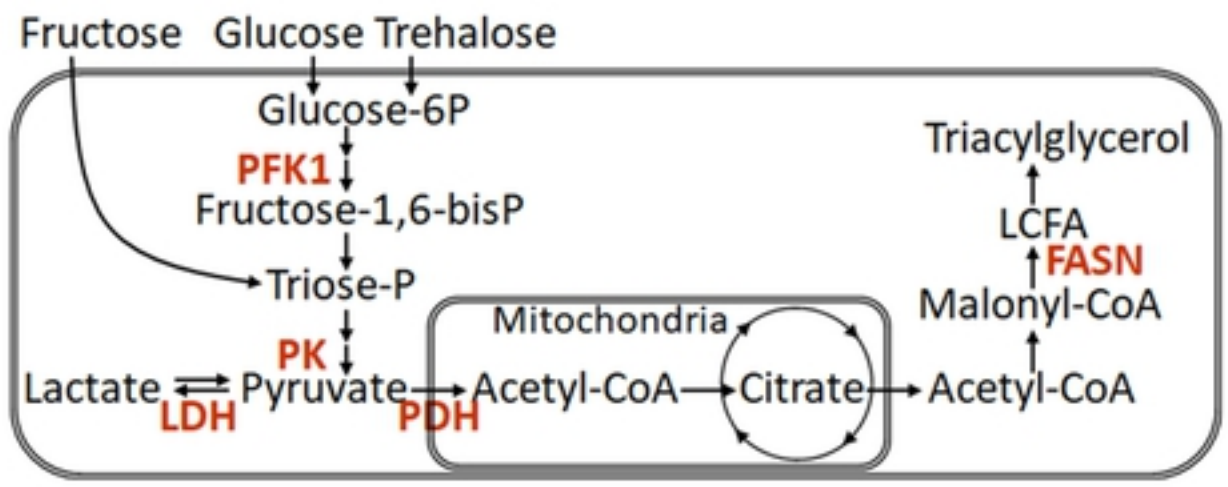


B

| 19°C>>29°C | 0h | 24h |
|---|---|---|
| PFK1-Ri | † L1/L2 | † late L2 |
| PK-Ri | † L2/L3 | † L3/pp |
| LDH-Ri | † L2/L3 | † L3/pp |
| PDH-Ri | ½† L3/pp | ½† L3/pp |

C

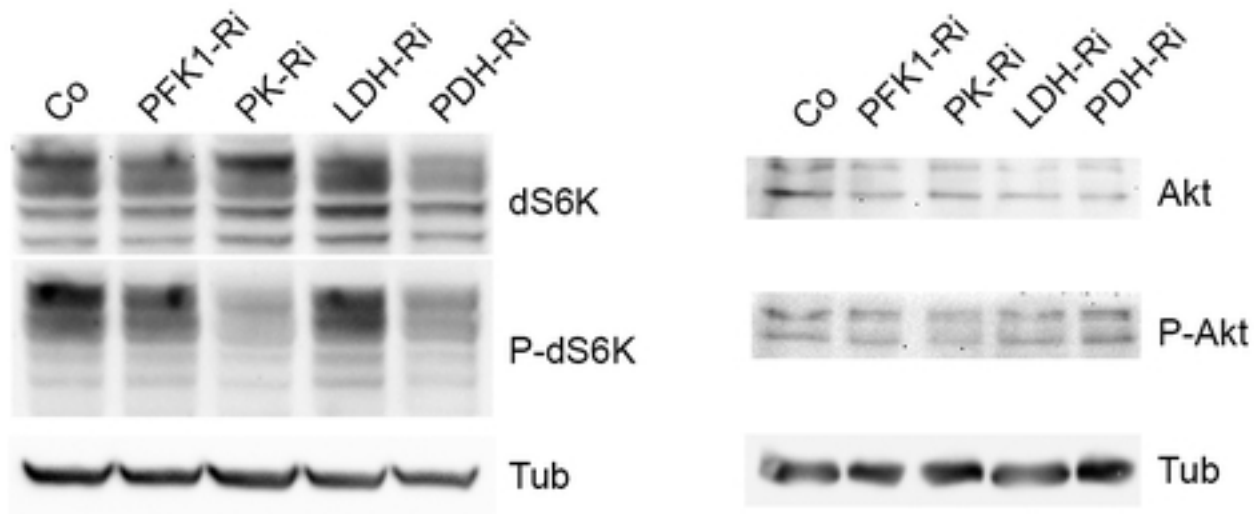


D

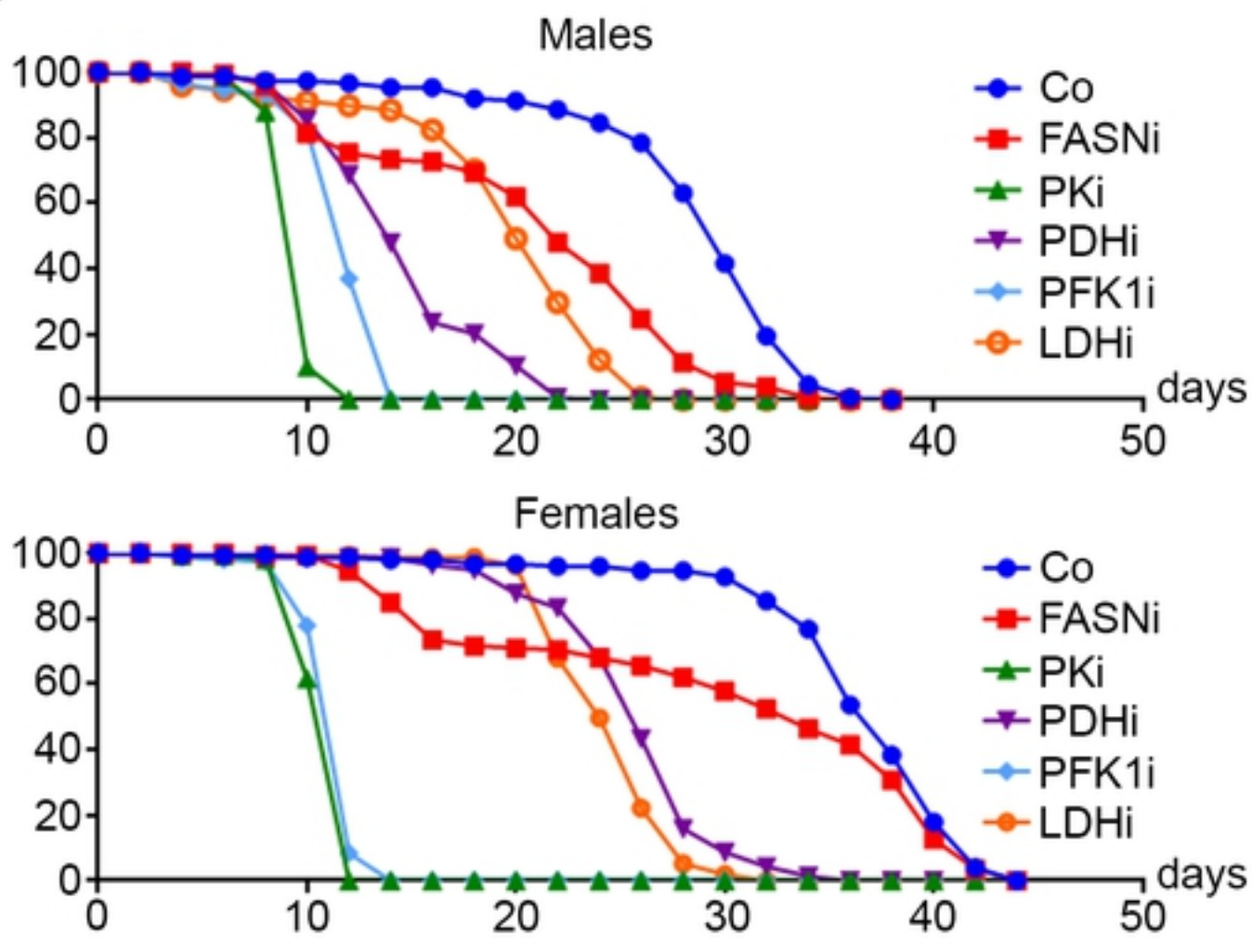


Figure 4